Journal of Electrical and Computer Engineering

Computational Intelligence and Heuristic Techniques in Microgrids

Lead Guest Editor: Emanuele Ogliari
Guest Editors: Minh Quan Duong, Trung Hung Vo, and Alessandro Niccolai

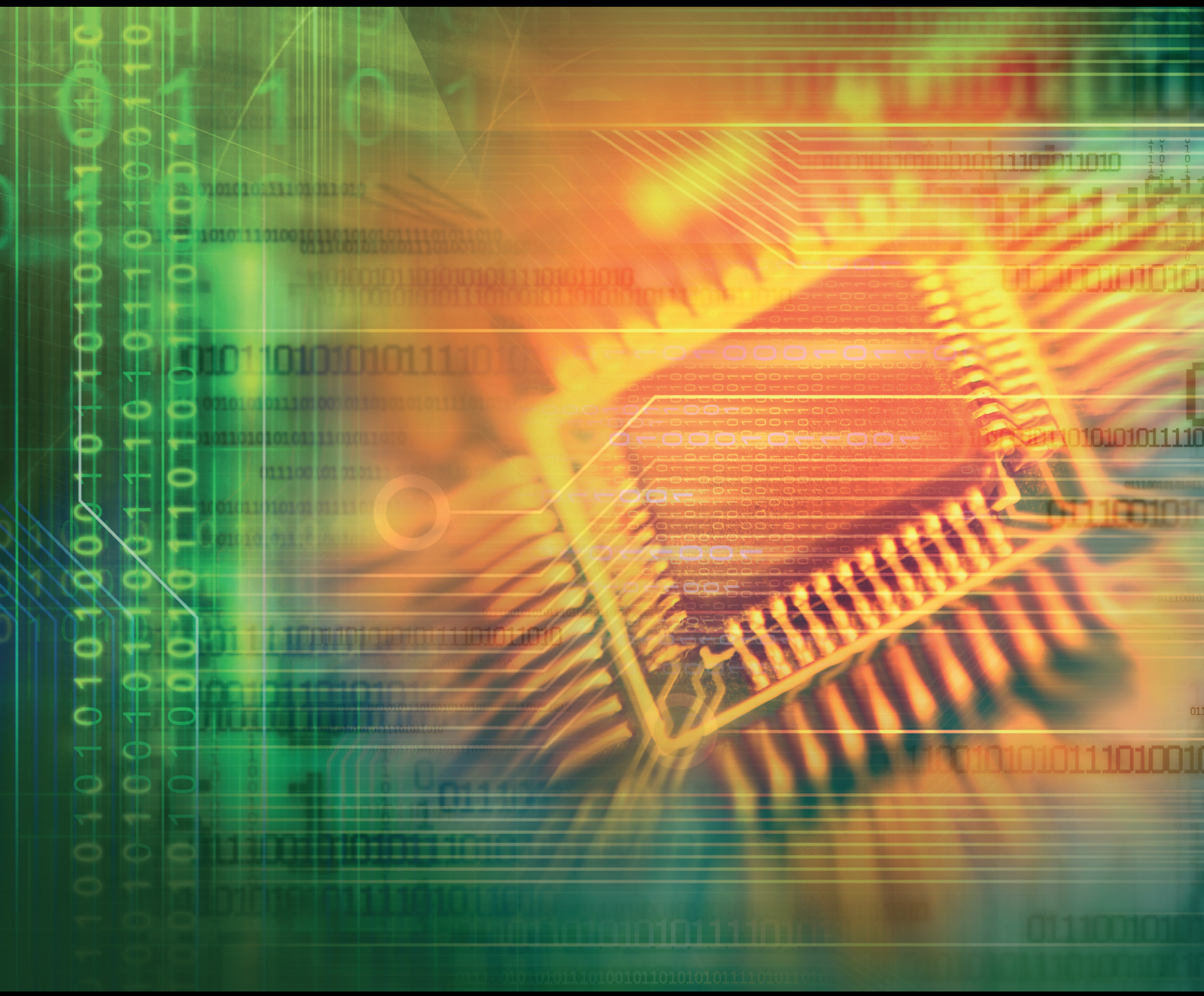

Computational Intelligence and Heuristic Techniques in Microgrids

Journal of Electrical and Computer Engineering

Computational Intelligence and Heuristic Techniques in Microgrids

Lead Guest Editor: Emanuele Ogliari
Guest Editors: Minh Quan Duong, Trung Hung Vo, and Alessandro Niccolai

Copyright © 2020 Hindawi Limited. All rights reserved.

This is a special issue published in "Journal of Electrical and Computer Engineering." All articles are open access articles distributed under the Creative Commons Attribution License, which permits unrestricted use, distribution, and reproduction in any medium, provided the original work is properly cited.

Circuits and Systems

Muhammad Taher Abuelma'atti, Saudi Arabia
Domenico Bianchi, Italy
Luca Cassano, Italy
Henry Chen, USA
M. Jamal Deen, Canada
Prince Jain, India
Jayshri Kulkarni, USA
Arjuna Madanayake, USA
Shibendu Mahata, India
Shun Ohmi, Japan
Susana Ortega-Cisneros, Mexico
Ping-Feng Pai, Taiwan
R. Palanisamy, India
Jose R. C. Piqueira, Brazil
Egidio Ragonese, Italy
Gabriel Robins, USA
Raj Senani, India
Vincenzo Stornelli, Italy
Ephraim Suhir, USA
Hannu A. Tenhunen, Finland
George S. Tombras, Greece
Suman Lata Tripathi, India
Gurvinder S. Virk, United Kingdom

Communications

Islam Abdellah, USA
Mominul Ahsan, United Kingdom
Bhargav Appasani, India
Nihal Areed, Egypt
Shonak Bansal, India
Francesco Benedetto, Italy
Giulio Maria Bianco, Italy
Yogesh Kumar Choukiker, India
René Cumplido, Mexico
Luca De Nardis, Italy
Rajesh Khanna, India
Kiseon Kim, Republic of Korea
Tho Le-Ngoc, Canada
Jit S. Mandeep, Malaysia
Montse Najar, Spain
John N. Sahalos, Greece
Vinod Sharma, India
Kuei-Ping Shih, Taiwan
Iickho Song, Republic of Korea
Sangeetha Subbaraj, India
Andrea Tani, Italy
George Tsoulos, Greece
Neng Ye, China

Power Systems

Hadi Nabipour Afrouzi, Malaysia
Ayman Al-Quraan, Jordan
Mahendra Bhadu, India
Antonio Bracale, Italy
Vito Calderaro, Italy
Vincenzo Di Dio, Italy
Salvatore Favuzza, Italy
Rajendra Kumar Khadanga, India
Alessandro Lidozzi, Italy
Giovanni Lutzemberger, Italy
Sheila Mahapatra, India
Luca Maresca, Italy
Antonio J. Marques Cardoso, Portugal
Fabio Massaro, Italy
Daniele Menniti, Italy
Manuela Minetti, Italy
Dillip Mishra, USA
Vitor Monteiro, Portugal
Nicola Pasquino, Italy
Luigi Piegari, Italy
Renato Procopio, Italy
Daniela Proto, Italy
Michele Riccio, Italy
Renato Rizzo, Italy
Gulshan Sharma, South Africa
Iouliia Skliarova, Portugal
Jayesh Soni, USA
Nicola Sorrentino, Italy
Kusum Verma, India
Chao Zhai, China

Signal Processing

Raid Al-Nima, Iraq
Aleksandar Dogandzic, USA
Martin Haardt, Germany
Jiri Jan, Czech Republic
Ramash Kumar K, India
Chi Chung Ko, Singapore
James Lam, Hong Kong
William Sandham, United Kingdom
Ravi Sankar, USA
Ari J. Visa, Finland
Gongping Yang, China

Contents

Hindawi
Journal of Electrical and Computer Engineering
Volume 2020, Article ID 9586707, 14 pages
https://doi.org/10.1155/2020/9586707

Research Article

The Importance of Distance between Photovoltaic Power Stations for Clear Accuracy of Short-Term Photovoltaic Power Forecasting

Abdelhakim El hendouzi,[1] **Abdennaser Bourouhou**,[2] **and Omar Ansari**[3]

[1]*Lab Research in Electrical Engineering, National School of Computer Science and Systems Analysis and Higher Normal School of Technical Education, Mohammed V University of Rabat, Avenue of the Royal Army, Madinat Al Irfane, District Riad, Rabat 100100, Morocco*
[2]*Lab Research in Electrical Engineering, Higher Normal School of Technical Education, Avenue of the Royal Army, Madinat Al Irfane, District Riad, Rabat 100100, Morocco*
[3]*Lab Research in Mechanical Engineering, Higher Normal School of Technical Education, Avenue of the Royal Army, Madinat Al Irfane, District Riad, Rabat 100100, Morocco*

Correspondence should be addressed to Abdelhakim El hendouzi; abdelhakim.elhendouzi@um5s.net.ma

Received 27 November 2019; Revised 18 February 2020; Accepted 2 March 2020; Published 10 April 2020

Guest Editor: Minh Quan Duong

Copyright © 2020 Abdelhakim El hendouzi et al. This is an open access article distributed under the Creative Commons Attribution License, which permits unrestricted use, distribution, and reproduction in any medium, provided the original work is properly cited.

The current research paper deals with the worldwide problem of photovoltaic (PV) power forecasting by this innovative contribution in short-term PV power forecasting time horizon based on classification methods and nonlinear autoregressive with exogenous input (NARX) neural network model. In the meantime, the weather data and PV installation parameters are collected through the data acquisition systems installed beside the three PV systems. At the same time, the PV systems are located in Morocco country, respectively, the 2 kWp PV installation placed at the Higher Normal School of Technical Education (ENSET) in Rabat city, the 3 kWp PV system set at Nouasseur Casablanca city, and the 60 kWp PV installation also based in Rabat city. The multisite modelling approach, meanwhile, is deployed for establishing the flawless short-term PV power forecasting models. As a result, the implementation of different models highlights their achievements in short-term PV power forecasting modelling. Consequently, the comparative study between the benchmarking model and the forecasting methods showed that the forecasting techniques used in this study outperform the smart persistence model not only in terms of normalized root mean square error (nRMSE) and normalized mean absolute error (nMAE) but also in terms of the skill score technique applied to assess the short-term PV power forecasting models.

1. Introduction

The reports by Renewables 2017 Global Status and International Energy Agency (IEA) confirmed that the solar PV power has grown tremendously which implied many economic and social benefits. The cumulative solar PV capacity, meanwhile, reached 398 GW which generated over 460 TWh and represented around 2% of global power energy [1]. However, the penetration of renewable energy particularly the solar PV remains trivial in comparison to the fuel and coal-fired power plants due to numerous technical and economic challenges. In this case, the need for high penetration of solar PV in power systems is chronic and required. The solar PV, meanwhile, depends on the weather parameters and the location of PV installation, which are unpredictable and affect the daily solar energy generation. However, in the case of solar PV grid-tied, the poor electrical grids cannot support this source of energy. For that reason, the strong penetration of solar PV energy in the global energy mix has driven the thinking to next generation of electrical power grids and the renovation of most existence electrical grids to host the new mode of solar PV and

guaranteeing its integration. In this case, the need to smart energy management systems (SEMS) that incorporate the forecasting methods of solar PV power is an important key to overcome many trials of renewable energy challenges and allow them (especially the PV power) the flexibility in terms of control and monitoring. Moreover, the forecasting methods can help the integration of natural and sustainable energy resources and encourage the adoption of recent energy systems such as microgrids, which are smart small microgenerations based on microsources including the renewable energy. The microgrids, meanwhile, request advanced techniques of control and forecasting to overcome the effect of solar PV variability. Also, the use of short-term PV power forecasting algorithms can support the integration of solar PV in microgrids by providing the profile of PV power for next 24 hours, which can aid the control flexibility, regulation, monitoring, and dispatching of microgrids. In addition, further advantages of PV power forecasting such as the economic returns which they are clear in the planning of energy generation, which supported by the demand forecasting. However, the elctricity cost optimization.

The current research article states the need for accurate short-term PV power forecasting due to its positive effect on scheduling. They can help the energy market operators escape the potential penalties due to the eccentricities between the planned and produced energies. This research study, meanwhile, suggests the best design of PV power forecasting model, which consisted on selecting the right future time horizon that means the choice of time between the current time and the needed future time, choosing the right forecasting resolution, and selecting the suitable forecasting approach. The time horizons mostly considered by the literature include very short term that starts from some seconds and ends in few minutes also includes the "time scale starts from several days to several months. In addition, the spatial horizon is also needed for PV power forecasting, which can display the total of space foreseen by the forecasting model; this forecasting horizon begins from one site to regional areas, also called regional forecast or multisite forecast [2]. Moreover, the need for forecasting approaches is primal for forecasting modelling. In the meantime, the survey of literature showed that the PV power forecasting is possible by using the direct and indirect techniques. The direct technique, meanwhile, resides on counting directly the amount of PV power in a future time horizon; also, the experts recommend the techniques of artificial intelligence and machine learning for short-term PV power forecasting. The indirect technique or solar irradiation forecasting consists on transforming the solar irradiation forecasting through a PV model to the PV power [3]. The literature review also recognized three main approaches for PV power forecasting modelling [4]. They include the physical approach based on real model of PV installation, the physical model, the rental of equipment, etc. The statistical approach includes methods belonging to the artificial intelligence, data mining, and machine learning. The hybrid approach is a new approach that gathers the techniques of different approaches or considers the collaboration between techniques of the same approach. Certainly, other approaches used for PV power forecasting include the time series, regressive, and probabilistic methods.

In the meantime, the literature review showed some related research articles in short-term PV power forecasting topic based on artificial neural networks and classification methods. In this case, the review article by Inman et al. [5] showed successful applications of solar forecasting methods and other theories related to the PV power resources and forecasting. The focus of this paper, meanwhile, is about the comparative study established between the artificial neural networks and K-nearest neighbors (KNNs), which both considered methods of artificial intelligence. The review article by Voyant et al. [6] presented a list of machine learning methods including the K-NN method which is considered as the groundwork for this current research paper. The research paper by Zamo et al. [7] presented a set of PV power forecasting methods called (PEARP). In the meantime, the focus of this study is about the use of data provided by 28 PV power plants, which encourage the use of data provided by multiple sites for feeding the forecasting models such as the case of this current research paper. The research study by Almonacid et al. [8] proposed multilayer perceptron neural network for forecasting the global irradiance and air temperature, alongside with NAR neural network that is used for calculating the PV power; however, the use of NAR did not take into account the effect of outputs on the forecasting results; nevertheless, the present research paper proposed NARX instead of NAR. The research article by Chu et al. [9] presented three smart models for reforecasting PV power; the models included the KNN; nevertheless, in their study, they did not combine the KNN method with any algorithm of similarity and thus it is very clear in their results. This present research paper is also inspired by the studies conducted by Li et al. and Gigoni et al. [10, 11] which presented some useful methods for data normalization and assessments for error minimization measured between the forecasted and real PV powers.

The context of this research paper is the contribution to resolve the dilemma of short-term PV power forecasting by the application of similarity algorithm (SA) with the KNN method and NARX neural network model applied to three different sites with varied sizes and distinct geographical locations. The forecasting model, meanwhile, consisted on choosing the right variables that fit more the pattern of PV power and then the use of artificial intelligence methods. The SA method, meanwhile, calculates the distance between the weather variables and PV system parameters. In addition, the KNN, which is a straightforward method, is used for short-term PV power forecasting with NARX neural network. The main goal of this research article, meanwhile, is contributing to the short-term PV power forecasting modelling. Also, this research article highlights the effect of distance between the PV power installations on short-term PV power forecasting by answering the need for optimal number of variables that fit more the PV power [12]. Moreover, the smart persistence model is used in this study as the benchmarking model of PV power forecasting.

The body of this research article contains the outline of PV system at Rabat ENSET School, which consists of a profound study of DC and AC installation, alongside the model of PV system. In the meantime, the highlight of equipment that used for measuring the weather and PV system parameter data. Moreover, the presentation of solar PV power forecasting methods explains the process of forecasting modelling as well as the contrast on useful equations and models used in this topic. Lastly, the demonstration of results and the perspectives are presented.

2. Outline of PV System at Rabat ENSET School

The purpose of this section is building the PV model of the PV system located at ENSET School. In this case, the PV model supports the PV power forecasting modelling since it allows the complete understanding of the PV system and the knowledge of important PV parameters. With the aim to facilitate the study of PV system, this research article considers the separation of DC and AC parts. In the meantime, the modelling of PV system starts from the study of the PV system location and the DC and AC materials. The PV system at ENSET School, meanwhile, availed for lighting. However, the extra power incorporates the electrical grid since the grid-tied inverter is used for the integration service as illustrated in Figures 1 and 2.

2.1. Overview of Geographical Characteristics of ENSET School Location. The ENSET School located in Rabat of Morocco benefits from an extraordinary site, which is most of the time sunny. For further information about the system location, Table 1 shows the geographical coordinates of the ENSET School site. This location holds a PV system of 2 kWp established by eight (8) PV panels installed in south facing as illustrated in Figures 3(a) and 3(b).

The ENSET PV system equipped by eight PV panels has the identical electrical features as shown in Table 2.

2.2. PV System Electrical Characteristics

2.2.1. PV System DC Parameters. The DC component of the PV system includes a metallic structure designed for eight PV modules, a DC junction box that contains the DC circuit breakers, and the electrical cables as shown in Figures 3(a) and 3(b). In the meantime, the serial configuration of PV panels is adopted with the aim to answer the input voltage required by the inverter. Furthermore, Table 3 provides further data about the PV array installed at the ENSET ground.

In this study, the single diode model is used for PV modelling. The implementation and simulation of the PV model, meanwhile, based on MATLAB software are shown in Figure 4. In addition, the PVSYST software used to simulate the voltage at the maximum power point tracking (MPPT) of the PV array, which is designed to provide the essential input voltage of the inverter, is illustrated in Figure 5.

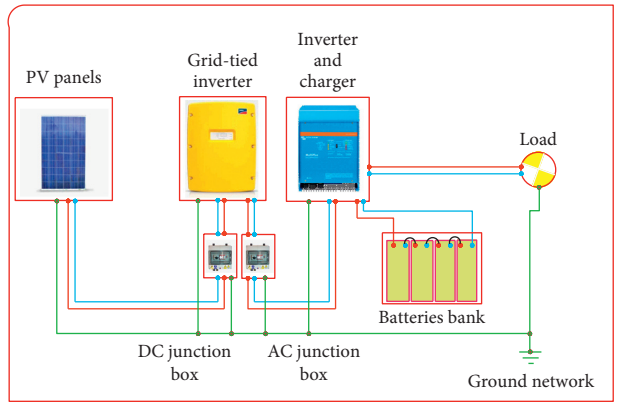

Figure 1: Synoptic diagram of the PV system at ENSET School; this one reflected the small-scale microgrid with the system of storage (batteries bank) and grid-tied inverter.

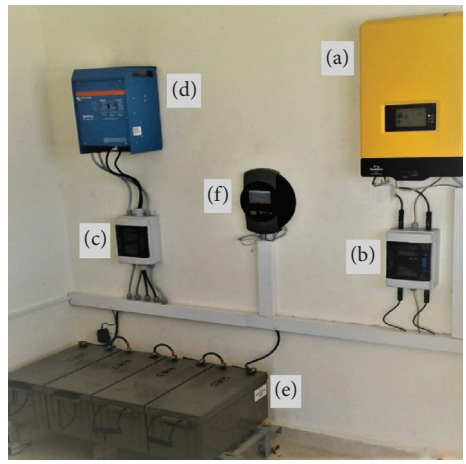

Figure 2: The photo of the DC and AC equipment of the PV system of 2 kWp located at Rabat city of Morocco. (a) The grid-tied inverter (SMA Sunny Boy 2000 HF). (b) The junction box for grid-tied part, which holds the circuit breaker. (c) The junction box for off-grid part, which contains the circuit breaker. (d) The inverter/charger, which is doted by the options of voltage control, battery charger, and inverter (Victron Energy). (e) The bank of waterproof gel batteries (12V-220 Ah) of Victron Energy brand. (f) The gear, which is used for monitoring the PV system and data registering (Solar Log 1200).

Table 1: The PV system geographical coordinates.

Site	City/country	Latitude	Longitude	Altitude (m)
ENSET School	Rabat/ Morocco	34.0°N	6.0°W	135

2.2.2. PV System AC Parameters. The second part of PV system modelling regards the AC kit, which covers an inverter, the AC junction box that contains the AC circuit breakers, and the electrical cables. Furthermore, the inverter used to convert the PV power provided by the PV array as well as to order the device of power limitation is shown in Figure 6. Table 4, meanwhile, provides further data about the AC part.

(a) (b)

Figure 3: ENSET School PV system. (a) The panels' orientation. (b) The panels' structure.

Table 2: The electrical characteristics of PV modules of the ENSET PV system.

Module PV	Si-poly
Manufacturer	Solar World
Model	SUNMODULE PLUS SW 250 POLY
Power at maximum point power pmpp(W)	250
Open circuit voltage V_{co} (V)	37, 6
Voltage at maximum point power V_{mpp} (V)	30, 5
Open circuit current Ico (A)	8, 81
Current at maximum point power I_{mpp} (A)	8, 27
Module efficiency (%)	14, 91%

Table 3: The DC parameters of the ENSET PV system.

PV modules in series	8
PV modules in parallel	N/A
Metallic structure	8
Tilt °	26
PV array area (m^2)	13, 4
PV module area (m^2)	11, 7
Array global power at nominal conditions (STC) kWc	2
Array global power at operating conditions (50°C) kWp	2, 13
Array operating characteristics (50°C) U_{mpp} (V)	256
Array operating characteristics (50°C) I_{mpp} (A)	8

2.2.3. Balances and Main Results. This part presents the main analysis of the energy produced by the whole PV system of the ENSET School over the year as shown in Figures 7 and 8. The energy over year, meanwhile, remains unpredictable and depends on the location of PV system and the days and the season of the year. Although, in Morocco, the daily energy for December and January months is less than other periods because this two months belong to the winter season. For further analysis in terms of losses of the energy provided by the ENSET PV system, the chart in Figure 9 illustrates the estimation of the PV system losses over the year, which is 10.3%.

2.3. Overview of the Monitoring Gear of the ENSET School PV System. The PV system at ENSET School includes a sensor network that embeds sensors of ambient temperature, module temperature, wind speed, and solar irradiance. The sensors can provide the data through RS485/422 cables or

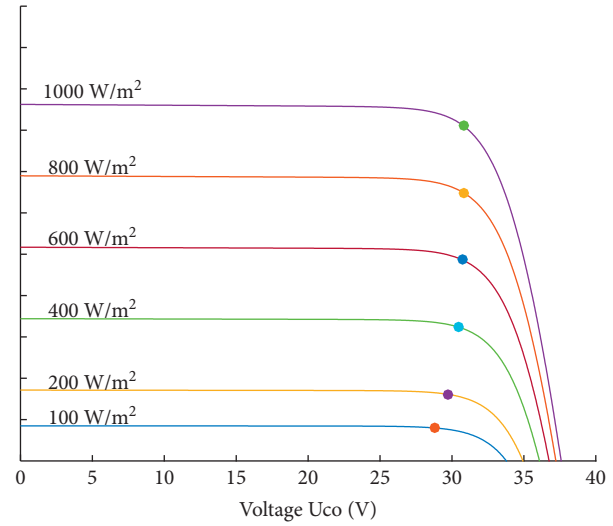

Figure 4: The IV curve provided by the model of the installed PV panel of brand SUNMODULE PLUS SW 250 POLY; the simulation used diverse values of plan of array irradiance (POA).

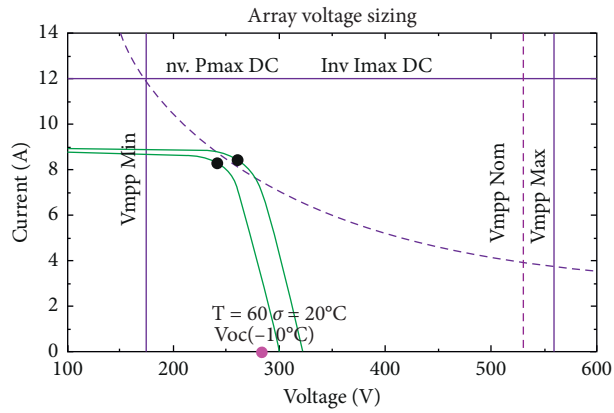

Figure 5: A snapshot view of the PV array at ENSET School. This architecture corresponds to the series configuration of PV modules since the value of array voltage is the total of the voltage of each individual PV module.

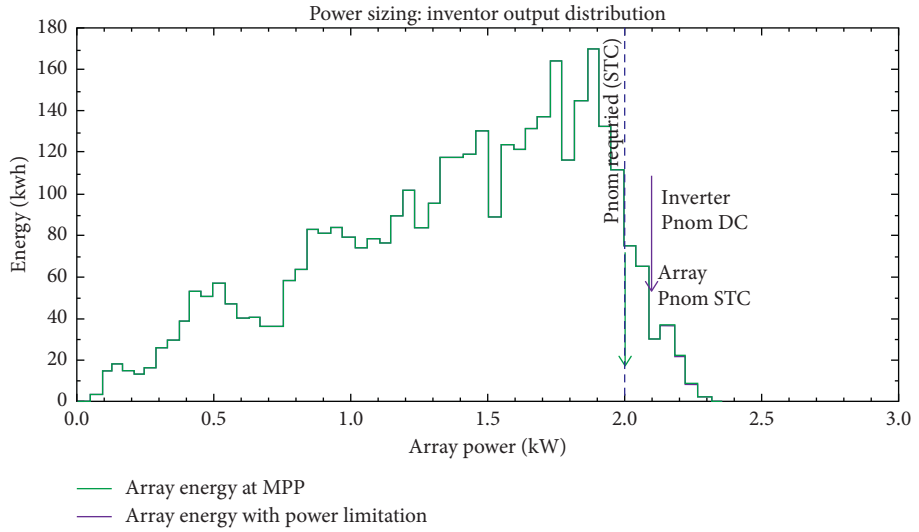

Figure 6: The energy distribution from the inverter, which depends on PV array voltage and current; in this case, the operating voltage of the inverter corresponds to 175–560 V.

Table 4: Recaps of simulation of ENSET's AC PV system.

Inverter	SMA
Model	Sunny Boy 2000 HF
Unit nominal power kW AC	2
Operating voltage (V)	175–560
Total nominal power kw AC	2
Produced energy kWh/year	3483
Specific production kWh/kWp/year	1741
Performance ratio PR (%)	90, 90%

Ethernet mode to the central data acquisition called solar log, which is able to communicate the data through the website and android application. The solar log's target, meanwhile, is ensuring the management and monitoring of the ENSET PV system including the visualization, optimization, and management process of self-consumption and grid-tied PV system. In the meantime, this equipment achieves the drop of power generation. At the same time, this equipment can ensure the limitation of reactive current through an installed external box.

However, with the aim of establishing the database for forecasting modelling, the website as well as the USB device used to export the data needs from the solar log in Excel files is illustrated by the diagram in Figure 10.

3. Data and Methods of Solar Photovoltaic Power Forecasting

3.1. Data Normalization. The standardization or data normalization corresponds to the process of scaling the data through mathematical equations. The data normalization, meanwhile, is worthwhile for the flawlessness of PV power forecasting models, for example, neural networks perform better when inputs have the appropriate scale. The Z-score is known as the best used normalization method, which corresponds to the number of standard deviations from the mean. Furthermore, the mean and standard deviation are used to calculate the Z-score of data.

3.1.1. Mean. Equation (1) provides the mathematical form for finding the mean value of a specified variable.

$$V_m = \frac{1}{n}\sum_{j=1}^{n} V_j, \tag{1}$$

where V_m is the mean value of the vector parameters V, n is the number of elements in V, and V_j is the j^{th} element in V.

3.1.2. Standard Deviation. The standard deviation provides the spreading of values. In addition, it is mostly practical to set the range of data [13]. In the case of total population, equation (2) provides the mathematical structure for calculating the standard deviation of a specified variable. Moreover, when the data are a sample, equation (3) is preferred.

$$\text{std}_1 = \sqrt{\frac{1}{n}\sum_{j=1}^{n}\left(V_j - V_m\right)^2}, \tag{2}$$

$$\text{std}_2 = \sqrt{\frac{1}{n-1}\sum_{j=1}^{n}\left(V_j - V_m\right)^2}, \tag{3}$$

where V_j is the j^{th} element in vector V and V_m is the mean value of V.

3.1.3. Z-Score. Equation (4) is used to calculate the Z-score value of a stated variable.

$$Z_{\text{score}} = \frac{V - V_m}{\text{std}}, \tag{4}$$

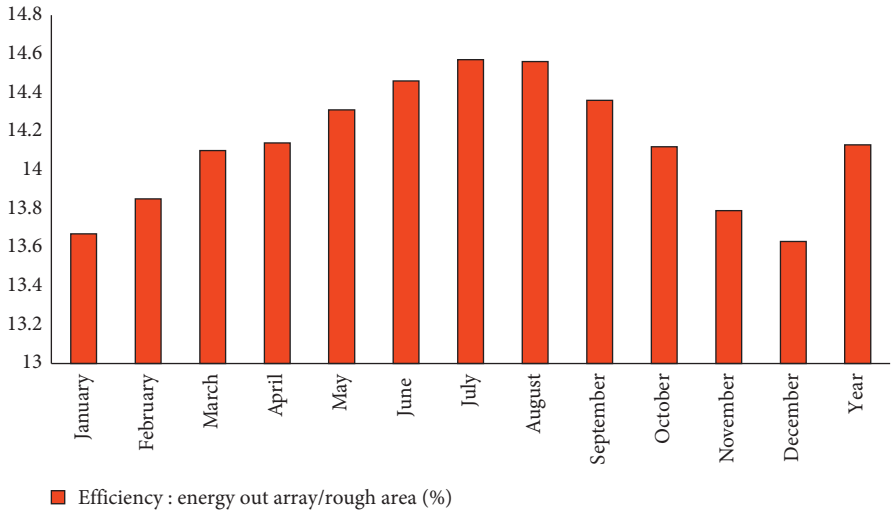

Figure 7: Assessment of ENSET PV array efficiency based on PVSYST software for each individual month of the year.

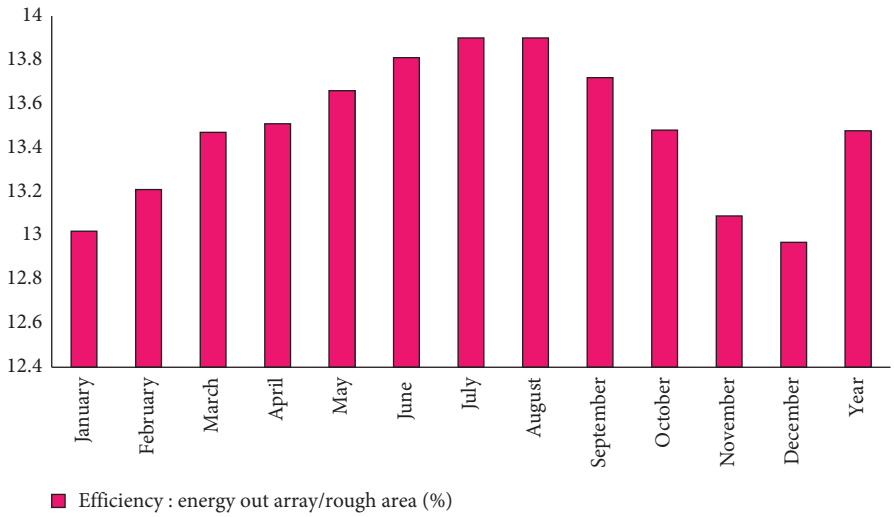

Figure 8: Assessment of ENSET PV array efficiency based on PVSYST software for each individual month of the year.

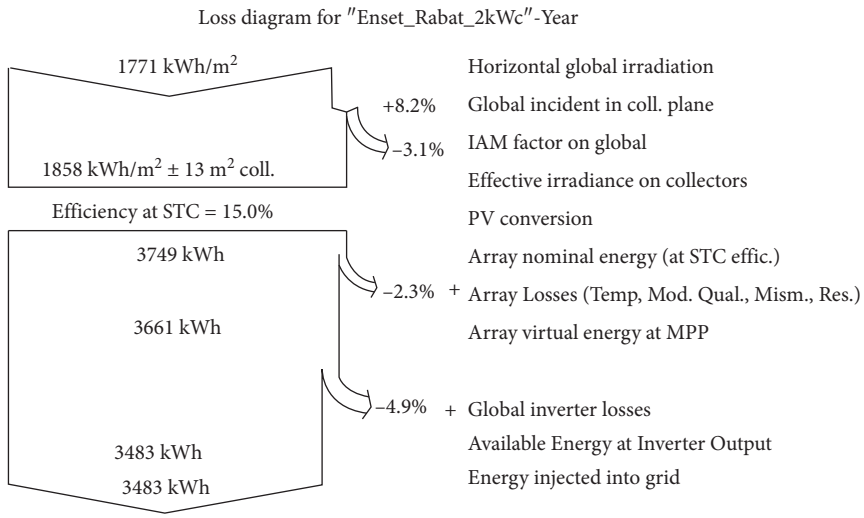

Figure 9: The loss diagram of the whole year for the ENSET PV system.

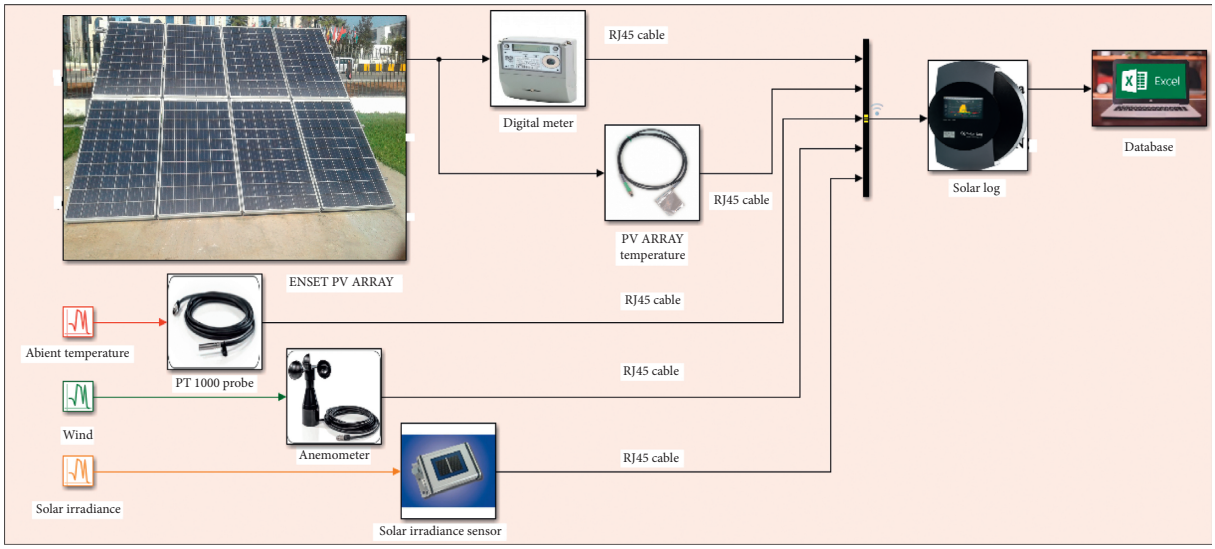

Figure 10: Solar log deployment for the ENSET School PV system.

where V is the vector of original values, V_m is the mean value of V, and std is the standard deviation of the data.

3.2. Physical Model of Photovoltaic Power Forecasting. The physical model of PV power forecasting is the most common one, which is based on the data measurement from both PV systems and weather stations [14].

3.2.1. Mathematical Expression of PV Power. The PV power produced by solar PV panels can be predictable by using a mathematical equation [15] as shown in the following equation:

$$P_{pv} = \xi \cdot S_m \cdot N \cdot I_{rr}, \tag{5}$$

where N is the number of solar PV panels, S_m is the surface of a solar PV module, I_{rr} is the solar radiation on the plan of PV module, and$\xi$is the instantaneous performance of the solar PV panel. The expression of ξ is shown in the following equation:

$$\xi = \xi_r \cdot \left(1 - \Gamma_{\text{tcstc}} \cdot \left(\Gamma_{\text{md}} - \Gamma_{\text{stc}}\right)\right), \tag{6}$$

where ξ_r is the reference efficiency of the PV module under STC conditions, Γ_{tcstc} is the temperature coefficient under STC conditions, which is a value given by the manufacturer, and Γ_{md} and Γ_{stc} are, respectively, the temperatures of the module at STC conditions and under any conditions.

3.2.2. Expression of Energy Irradiance. The effective irradiance received by the PV cell can be calculated by using the following equation:

$$I_{rr} = I_{\text{eff}} + \nabla_d \left(I_{dc} + I_{rs}\right), \tag{7}$$

where I_{eff} is the efficient irradiance, I_{dc} is the energy irradiance diffused by the sky, I_{rs} is the energy irradiance reflected from the ground, and ∇_d is the fraction of diffuse.

3.2.3. Mathematical Expression of SANDIA Cell Temperature Model. The Sandia Energy first proposed the SANDIA cell temperature model as a part of the Sandia PV system performance model [16]. Equation (8) meanwhile, calculates the temperature of PV module in degrees Celsius (C).

$$\Gamma_{\text{md}} = I_{rr} \cdot e^{a+b.ws} + \Gamma_{at}, \tag{8}$$

where a and b are the temperature coefficients, ws is the wind speed, and Γ_{at} is the ambient temperature.

In the meantime, the temperature of PV cell in degrees Celsius is available by using

$$\Gamma_{\text{celpv}} = \Gamma_{\text{md}} + \frac{I_{rr}}{1000}\alpha_t, \tag{9}$$

where α_t is a coefficient of temperature.

3.3. Correlation of Calculated and Measured Data. The PV power measured from the PV system is totally different from the PV power calculated by a PV model according to [17]. In the meantime, the PV power calculated by a PV model is equal to the PV power measured multiplied by a coefficient λ_{pow} as shown in the following equation:fd10

$$P_{\text{cal}} = \lambda_{\text{pow}} \cdot P_{\text{real}}. \tag{10}$$

The similar analysis above is practical for calculating the temperatures as shown in the following equation:fd11

$$\Gamma_{\text{md}} = \lambda_{\text{temp}} \cdot \Gamma_{\text{real}}. \tag{11}$$

3.4. Artificial Neural Networks (ANNs). Machine learning (ML) and artificial intelligence are considered as the advanced techniques since they allow the easy classification and forecasting of data. The ML includes the ANNs. Their objective is asking the machine to classify the data by splitting, but sometimes the error revealed the presence of misclassified data. Therfore, the aim of error function is getting the information about the misclassified data and also modelling the

error. The error function meanwhile is either discrete which is convenient for the classification problems or continuous which is suitable for the optimization problems. In the meantime, the gradient descent is applicable for minimization criteria. The probability is also used to describe the error function since the product of probabilities defines this function. Therefore, the existence of times of probabilities revealed that there is no error, and the maximum likelihood is determined. Moreover, the error function is guilty for the choice of right activation function in the ANNs modelling.

In this paper, the NARX neural network is used with feedback or closed loop architecture with time delay for both external inputs and feed-forwards from outputs as shown in Figure 11. The closed loop also called parallel architecture, meanwhile, is convenient for multistep PV power forecasting [18]. In this item, the NARX neural network with two layers is applied for short-term PV power forecasting model as well as used to contribute in the flawlessness of PV power forecasting.

3.5. Classification of Weather and PV System Parameters. The process of classification of weather variables and PV system parameters is useful to distinct the variables that fit more the pattern of measured PV power and to classify them according to their importance as primary, secondary, etc. This process realized through computer algorithms is based on mathematical equations such as the Euclidian distance, root mean square Euclidian distance difference, and weighted hybrid distance. The Euclidian distance, meanwhile, is used to calculate the distance between the elements of PV power vector and the elements of other variables. In the meantime, the root mean square Euclidian distance differences are used to cut the prime variable and the weighted hybrid distance is used to compute the rank of other external variables. In this paper, the classification rank is six variables.

Equation (12) is practical for calculating the Euclidian distance between the elements of PV power vector for days d and $d+1$.

$$D\left(v_j, d, d'\right) = \sqrt{\sum_{t=1}^{\tau}\left(P_t^{(d)} - P_t^{(d')}\right)^2}. \tag{12}$$

Furthermore, equation (13) is useful to compute the Euclidian distance between the elements of other variables for days d and $d+1$.

$$D\left(v_j, d, d'\right) = \sqrt{\sum_{t=1}^{\tau}\left(v_{j,t}^{(d)} - v_{j,t}^{(d')}\right)^2}. \tag{13}$$

However, to cut the prime external variable, the algorithm should organize the variables that fit more the PV power pattern by calculating the root mean square Euclidian distance differences ($\mathfrak{J}$) as shown in the following equation:

$$\mathfrak{J}\left(P, v_j\right) = \sqrt{\frac{\sum_{d'=2}^{n}\sum_{d=1}^{d'-1}\left(D\left(P, d, d'\right) - D\left(v_j, d, d'\right)\right)^2}{(1/2)n\cdot(n-1)}}, \tag{14}$$

where $(1/2)n\cdot(n-1)$ corresponds to the distance size and n is the variable dimension.

In addition, to discover the rank of other external variables, the weighted hybrid distance (ζ) and the root mean square weighted hybrid distance differences (ζ_Δ) are calculated for the Euclidian distance of the prime external variable and the Euclidian distance of other variables for days d and $d+1$ as shown in equations (15) and (16).

$$\zeta\left(v_j, d, d'\right) = \left(1-\gamma_{vj}\right)D\left(R_{v1}, d, d'\right) + \gamma_{vj}D\left(v_j, d, d'\right), \tag{15}$$

$$\zeta\left(R_{v2}, d, d^f\right) = \left(1-\gamma_{Rv2}\right)D\left(R_{v1}, d, d^f\right) + \gamma_{Rv2}D\left(R_{v2}, d, d^f\right), \tag{16}$$

where R_{vj} is the j^{th} label of the variable found by the similarity algorithm and γ_{vj} is a coefficient whose value is chosen as the smallest. In the perspective of this article, the algorithm of similarity is applicable to the data provided by the three sites that are previously discussed.

3.6. Approximate Method for Information Extraction from the Data. The question there is how one can sort the forecasted day from forecasting result. The extraction of the forecasted day is going to be hard when big data are available. In the meantime, equations (17) and (18) below are practical and helpful for finding the corresponding day and month in the forecasting result. Equation (17) is developed to sort the forecasted day from big data and finds its label in months of year.

$$\Delta_f = \frac{f_d}{N_{dy}}, \tag{17}$$

where Δ_f is the month of year, f_d is the forecasted day, and $N_{dy} = 30.42167$ corresponds to the average of 365 days of year. The result given by equation (17) is often with a comma where the decimal part corresponds to the month and the fractional part corresponds to the day of month.

Furthermore, equation (18) is practical to find the sorting of similar days to the forecast day.

$$\Delta_s = \frac{S_d}{N_{dy}}, \tag{18}$$

where Δ_s is the month of year. The outcome given by this equation has often a decimal part that corresponds to the month, and the fractional part corresponds to the day of month.

3.6.1. Example. The detected day by the algorithm of similarity is $f_d = 324$ and $\Delta_f = 10.652$. Therefore, the result corresponds to the month October and the fractional part 0.652 timed by the coefficient N_{dy} matches the day 20. Finally, the forecast day corresponds to 20 October.

3.7. Error Metrics of PV Power Forecasting. The mean absolute error (*MAE*) and root mean square error (*RMSE*) are mostly relevant and practical methods for assessing the

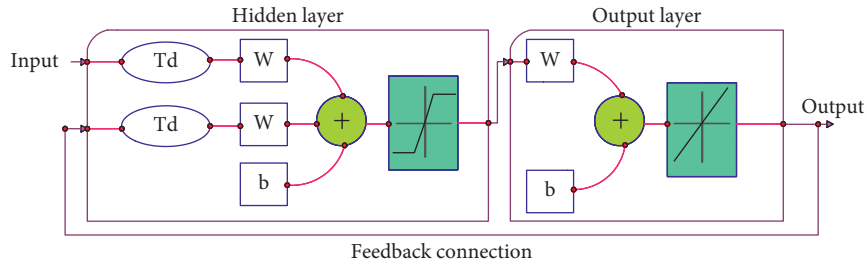

Figure 11: NARX neural network general scheme.

accuracy of PV power forecasting models [3]. The *MAE*, meanwhile, is used for finding the steady distance between the real and the outputted values from forecast models. Therefore, the *MAE* is appropriately practical for estimating the persistent forecast errors, whereas the *RMSE* deals with severely large errors in square order. Equations (19) and (20) show, respectively, the structure of *MAE* and *RMSE*.

$$\mathrm{MAE} = \frac{1}{n}\sum_{j=1}^{n}\left|P_{\mathrm{for}} - P_{\mathrm{real}}\right|, \tag{19}$$

$$\mathrm{RMSE} = \sqrt{\frac{1}{n}\sum_{j=1}^{n}\left(P_{\mathrm{for}} - P_{\mathrm{real}}\right)^2}, \tag{20}$$

where P_{for} is the forecasted PV power and P_{real} is the measured PV power.

However, to compare results generated from forecast models, the skill score Δ_f is the most practical method [19]. Equation (21) shows the structure of skill score technique.

$$\Delta_{sk} = 1 - \frac{Mf_x}{Mf_z}, \tag{21}$$

where Mf_x corresponds to the result from the forecasting model j and Mf_z corresponds to the result from the model $j+1$.

4. Results and Discussion

4.1. Simulation Results. This research paper provides the best results based on simulation of two kinds of model that belong to two different areas of artificial intelligence modelling. The first part of simulation concerns the results of artificial neural network application, specifically the use of NARX neural network model, and the second part of simulation concerns the application of classification methods, specifically the use of K-nearest neighbors with similarity algorithm to forecast the short-term PV power.

4.1.1. Weather and PV System Data. The building of database is the key process of forecasting modelling, and it has taken more time than expected. In the case of PV power forecasting study, two kinds of data can be initiated which are the weather data from meteorological stations and the PV system data measured directly from PV systems. In addition, for the subject of this research paper, the data used to feed the PV power forecasting models correspond to three different locations characterized by size dissimilarity. In the meantime, the PV system data at ENSET School provide 2247 hours of weather and PV system data; besides, the Casablanca and Rabat sites provide 8760 hours of weather and PV system data. Furthermore, the PVGIS which is a platform of weather data from the European Commission is used to provide other meteorological data from 2007 to 2016 for each site which they also used to feed the forecasting process as shown in Table 5 [20]. The platforms Excel, *R*, and MATLAB were used to create the database and implementing different forecasting models.

4.1.2. NARX Neural Network for PV Power Forecasting. The NARX neural network model is applicable for both weather and PV system data provided by the locations described above. In the meantime, the implementation of NARX pursues the separation or multimodel approach that means the implementation of NARX model for each individual site.

(1) NARX Forecasting Model for 2 kWp PV Power Station. The implementation of NARX forecasting model on ENSET School PV system and PVGIS weather data for the chosen days 25, 26, and 27 February shows satisfactory results that are clear by the PV power curves as presented in Figure 12. The NARX model of the ENSET PV system, meanwhile, contains three (3) hidden neurons.

(2) NARX Forecasting Model for 3 kWp PV Power Station. The implementation of NARX model of PV system on Casablanca (3 kWp) PV system shows satisfactory results for the chosen days 27, 28, and 29 November, which are clear by the PV power curves as shown in Figure 13. In this path, the NARX neural network model contains eleven (11) hidden neurons.

(3) NARX Forecasting Model for 60 kWp PV Power Station. The NARX neural network model applied to forecast the quantity of PV power (60 kWp) of another site located at Rabat city illustrates satisfactory results for the chosen days 27, 28, and 29 November as shown by the PV power curves in Figure 14. In the meantime, the NARX model contains fourteen (14) hidden neurons.

Therefore, the best performance of NARX is taken from the epoch with the lowest validation error. The NARX

Table 5: Summary of locations and input/output sizes used to feed the forecasting models.

Sites	Input variables	Output variables
Rabat 60kWp	8760×82	8760×1
Casablanca 3kWp	8760×82	8760×1
Rabat 2Kwp	2247×82	2247×1

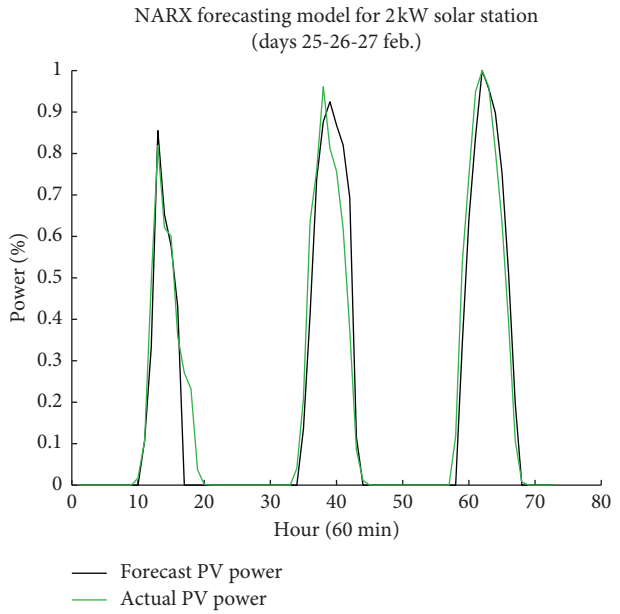

Figure 12: NARX neural network for forecasting days 25, 26, and 27 February of the year.

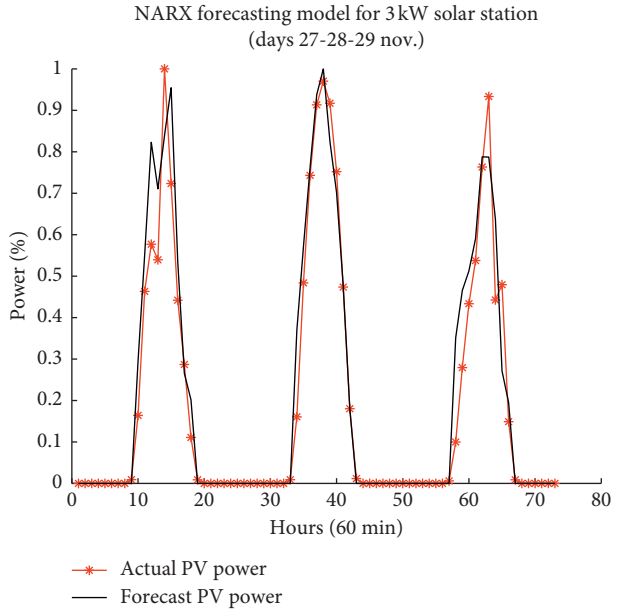

Figure 13: NARX neural network for forecasting days 27, 28, and 29 November of the year.

forecasting model, meanwhile, revealed perfect results in terms of skill scores in comparison with the smart persistence model as shown in Table 6. The use of straightforward

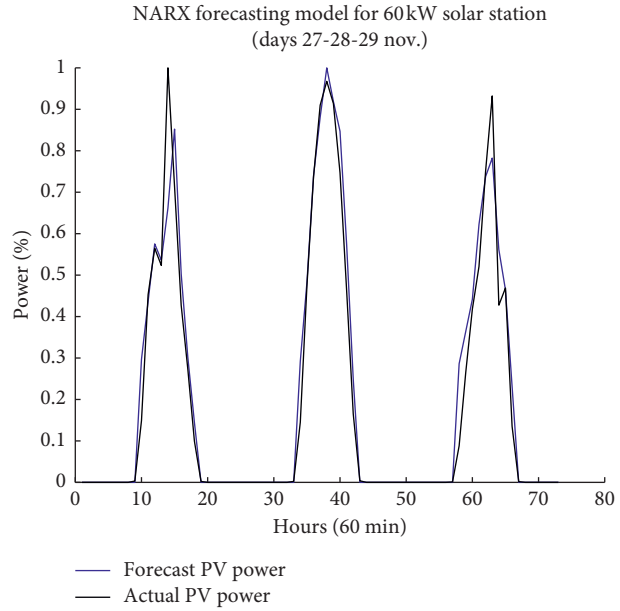

Figure 14: NARX neural network for forecasting days 27, 28, and 29 November of the year.

ANNs such as the NARX model for PV power forecasting shows excellent results. Nevertheless, the process of forecasting by NARX model takes more time such as the time allowed to the data preparation and standardization. In addition, the presence of some slighted outliers stresses the NARX neural network models and reduces their efficiency, which drives the thinking to other methods.

4.1.3. Similarity Algorithm and KNN for PV Power Forecasting. The first part of this approach concerns the algorithm of similarity that is based on root mean squared difference distances$\mathfrak{I}$, which is used to detect the similar days to the forecast day. The variable with the lowest $\mathfrak{I}$ is ordered as the prime external variable. The other variables are classed regarding their calculated root mean square weighted hybrid difference distances ζ_Δ. The second part uses the KNN model to forecast the short-term PV power.

In addition, the proposed forecasting process uses the same data shown in Table 5 for feeding the models of different locations. In the meantime, this research paper considers six external variables chosen by the similarity algorithm for each individual site as presented, respectively, in Table 7 for the 2 kWp PV station, Table 8 for the 3 kWp PV station, and Table 9 for the 60 kWp PV station.

Furthermore, the simulation results for both classification and forecasting noticeably present best results as shown, respectively, in Figure 15 for the 20 February forecasting day of the 2 kWp PV system, Figure 16 for the 26 September forecasting day of the 3 kWp PV system, and Figure 17 for the 7 July forecasting day of the 60 kWp PV system. The result summary of the similarity algorithm is shown in Table 10.

Therefore, the KNN forecasting model presents satisfactory results in terms of skill scores in comparison with the

Table 6: Summary of accuracy assessment of NARX neural network forecasting model for each location.

Metrics/Locations	Rabat 60kWp	Rabat 2kWp	Casablanca 3kWp
$RMSE_{NARX\ 27}$ (%)	10.145	—	11.178
$RMSE_{PERSISTENCE\ 27}$ (%)	23.339	—	22.887
$\Delta_{sk_{RMSE27}}$(%)	0.565	—	0.511
$MAE_{\ NARX\ 27}$ (%)	5.130	—	8.333
$MAE_{PERSISTENCE\ 27}$ (%)	15.642	—	15.448
$\Delta_{sk_{RMSE27}}$(%)	0.672	—	0.460
$RMSE_{NARX\ 28}$ (%)	5.948	—	6.570
$RMSE_{PERSISTENCE\ 28}$ (%)	15.570		15.098
$\Delta_{sk_{RMSE28}}$(%)	0.617	—	0.564
$MAE_{\ NARX\ 28}$ (%)	3.508	—	3.593
$MAE_{PERSISTENCE\ 28}$ (%)	9.297	—	9.041
$\Delta_{sk_{RMSE28}}$(%)	0.622	—	0.602
$RMSE_{NARX\ 29}$ (%)	8.036	—	11.178
$RMSE_{PERSISTENCE\ 29}$ (%)	16.261	—	15.763
$\Delta_{sk_{RMSE29}}$(%)	—	—	—
$MAE_{\ NARX\ 29}$ (%)	4.841	—	7.082
$MAE_{PERSISTENCE\ 29}$ (%)	9.210	—	8.977
$\Delta_{sk_{RMSE29}}$(%)	0.474	—	0.211
$RMSE_{NARX\ 25}$ (%)	—	10.043	—
$RMSE_{PERSISTENCE\ 25}$ (%)	—	75.119	—
$\Delta_{sk_{RMSE25}}$(%)	—	0.866	—
$MAE_{\ NARX\ 25}$ (%)	—	5.491	—
$MAE_{PERSISTENCE\ 25}$ (%)	—	79.015	—
$\Delta_{sk_{MAE25}}$(%)	—	0.930	—
$RMSE_{NARX\ 26}$ (%)	—	12.099	—
$RMSE_{PERSISTENCE\ 26}$ (%)	—	17.641	—
$\Delta_{sk_{RMSE26}}$(%)	—	0.314	—
$MAE_{\ NARX\ 26}$ (%)	—	7.699	—
$MAE_{PERSISTENCE\ 26}$ (%)	—	11.412	—
$\Delta_{sk_{MAE26}}$(%)	—	0.325	—
$RMSE_{NARX\ 27}$ (%)	—	8.945	—
$RMSE_{PERSISTENCE\ 27}$ (%)		11.212	—
$\Delta_{sk_{RMSE27}}$(%)	—	0.202	—
$MAE_{\ NARX\ 27}$ (%)	—	6.393	—
$MAE_{PERSISTENCE\ 27}$ (%)	—	6.688	—
$\Delta_{sk_{MAE27}}$(%)	—	0.044	—

Table 7: Classification of variables according to $\mathfrak{F}$ and ζ_Δ for 2 kWp PV power station.

R_{vj}	v_j	γ	$\mathfrak{F}$	ζ_Δ
R_{v1}	Module temperature (ENSET)*	—	0.005508720545916	—
R_{v2}	Relative humidity (R76)**	10^{-5}	—	0.019802673656454
R_{v3}	Wind direction (R76)	10^{-6}	—	0.019802837275625
R_{v4}	Ambient temperature (R76)	10^{-7}	—	0.019802846771643
R_{v5}	Ambient temperature (ENSET)	10^{-8}	—	0.019802847417763
R_{v6}	Direct normal irradiance (R76)	10^{-9}	—	0.019802847479204

**R76: weather data from 2007 to 2016 of Rabat. *ENSET: data of 2018 from ENSET School location at Rabat.

Table 8: Classification of variables according to $\mathfrak{F}$ and ζ_Δ for 3 kWp PV power station.

R_{vj}	v_j	γ	$\mathfrak{F}$	ζ_Δ
R_{v1}	Ambient temperature (NC)*	—	0.005508720545916	—
R_{v2}	Module temperature (NC)	10^{-5}	—	0.001322625296966
R_{v3}	Relative humidity (C76)**	10^{-6}	—	0.001322639903851
R_{v4}	Wind speed (C76)	10^{-7}	—	0.001322641151184
R_{v5}	Direct normal irradiance (C76)	10^{-8}	—	0.001322641234634
R_{v6}	Ambient temperature (C76)	10^{-9}	—	0.001322641242248

**C76: weather data from 2007 to 2016 of Casablanca. *NC: data from Nouasseur location at Casablanca.

Table 9: Classification of variables according to $\mathfrak{I}$ and ζ_Δ for 60 kWp PV power station.

R_{vj}	v_j	γ	$\mathfrak{I}$	ζ_Δ
R_{v1}	Ambient temperature (Rabat)**	—	0.0007698674850908259	—
R_{v2}	Module temperature (Rabat)	10^{-5}	—	0.001365317131326
R_{v3}	Relative humidity (R76)*	10^{-6}	—	0.001365332792013
R_{v4}	Wind speed (R76)	10^{-7}	—	0.001365334030451
R_{v5}	Direct normal irradiance (R76)	10^{-8}	—	0.001365334123127
R_{v6}	Wind direction (R76)	10^{-9}	—	0.001365334131037

**Rabat: data from a PV installation of 60 kWp location at Rabat. *R76: weather data from 2007 to 2016 of Rabat.

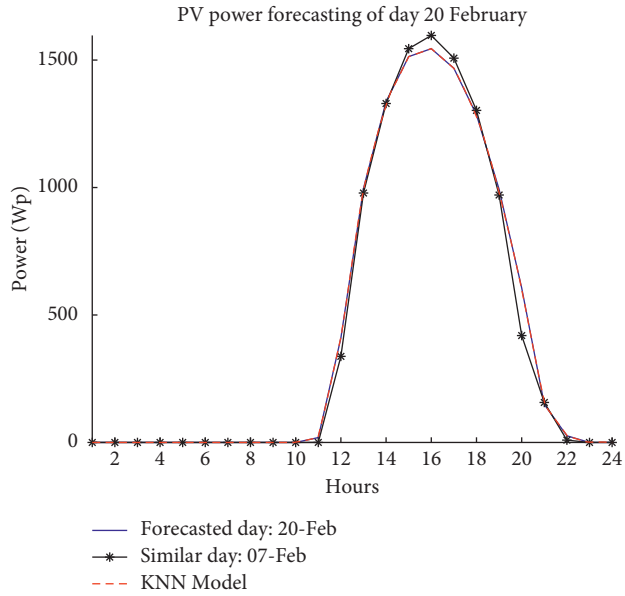

Figure 15: Similarity algorithm combined with KNN for forecasting the PV power of 20 February.

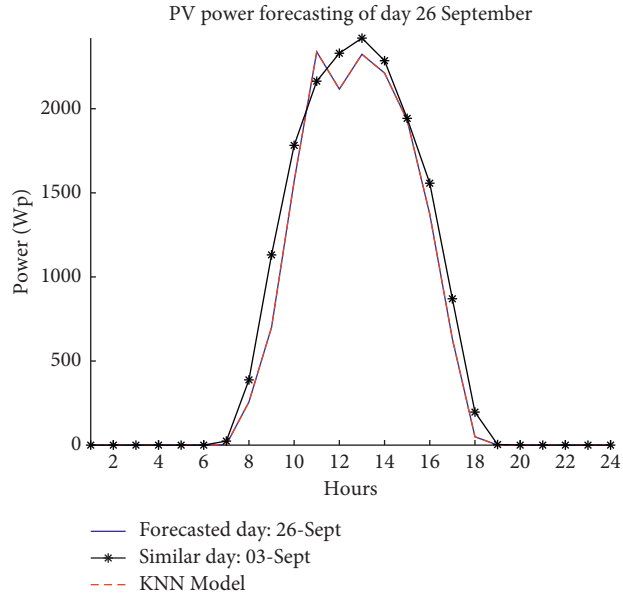

Figure 16: Similarity algorithm combined with KNN for forecasting the PV power of 26 September.

persistence model as shown in Table 11. The K is chosen equal to one (1) since in this simulation, just one day is detected as similar to the forecast day.

4.2. Discussion and Outlines. In the first case, the contribution in short-term PV power forecasting through the employment of classification techniques and artificial neural

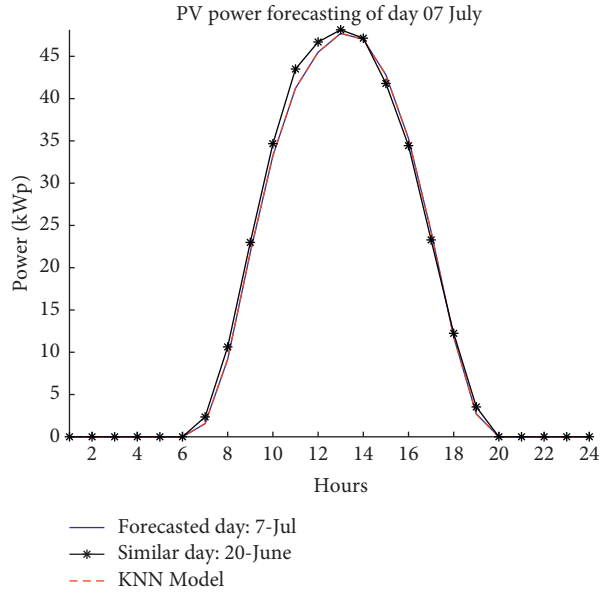

Figure 17: Similarity algorithm combined with KNN for forecasting the PV power for 7 July.

Table 10: Summary results of assessment of accuracy of similarity algorithm for each location.

Site	Forecasted day index	Similar day index	RMSE (%) sim	MAE (%) sim
Rabat 60 kWp	07-Jul	20-Jun	2.307	2.119
Casablanca 3 kWp	26-Sept	03-Sept	7.357	5.782
Rabat 2 kWp	20-Feb	07-Feb	4.450	2.858

Table 11: Summary results of assessment of accuracy of KNN forecast model for each location.

Metrics/Locations	Rabat 60 kWp	Rabat 2 kWp	Casablanca 3 kWp
$RMSE_{KNN}$ (%)	0	0	0
$RMSE_{PERSISTENCE}$ (%)	2.808	31.010	9.125
$\Delta_{sk_{RMSE-KNN}}$(%)	1	1	1
MAE_{KNN} (%)	0	0	0
$MAE_{PERSISTENCE}$ (%)	2.224	29.838	6.717
$\Delta_{sk_{MAE-KNN}}$ (%)	1	1	1

networks. Although, the both approaches are belonging to the artificial intelligence and machine learning. In the meantime, the KNN with similarity algorithm and NARX neural network models is established for each individual PV power system described in the aforementioned sections.

The forecasting system showed satisfactory results due to the use of similarity algorithm for selecting the significant variables, which means the classification of variables that fit more pattern of PV power. Hence, this process of selection decreases the time of modelling.

Moreover, the application of KNN method combined with the similarity algorithm revealed perfect results in comparison to the benchmarking model as well as the application of NARX neural network for short-term PV power forecasting. The NARX neural network, meanwhile, is a robust and powerful model since it takes into account the effect of outputs that feed-forwarded to inputs (see Figure 11). Nevertheless, it needs huge size of data that are used particularly for training, testing, and validation. For that reason, the NARX model is applied to the overall data of each individual location.

Consequently, the classification methods showed perfect results in terms of modelling simplicity in comparison to the artificial neural network models that suffer from the overfitting and memorization problems, even though data normalization performs well. In short, this research article recommends the process of similarity algorithm associated with KNN as the flawless short-term PV power forecasting model.

In the second case, the research article has proven the effect of distance between PV systems on short-term PV power forecasting modelling. The examination of results, meanwhile, has shown that the similarity algorithm must be employed to the weather and PV system parameters of each individual site even if the sites belong to the same geographical location (e.g., in this study, Rabat city covers two PV systems, 2 kWp and 60 kWp, respectively). However, the distance between PV system locations is an important parameter. Therefore, this confirmation is very significant when there is a need for multisite PV power forecasting modelling.

5. Conclusions

As a conclusion, firstly, this research article shows best results from the use of NARX and KNN methods. Therefore,

this present research article recommends the practice of classification techniques such as KNN combined with similarity algorithm for flawless short-term PV power forecasting. Furthermore, the optimization of forecasting modelling by selecting the optimal parameters is required since the choice of optimal variables that fit more the pattern of PV power can lead to forecasting error minimization and improving the forecasting accuracy. Secondly, this research article presents the effect of distance between PV power installations on PV power forecasting process. Therefore, this new parameter needs more studies and developments to show its real effect on forecasting models.

For future work, the advanced neural networks with optimization methods will be able to give a further solution to the dilemma of short-term PV power forecasting, as well as the consideration of other variables and parameters.

Data Availability

The data used to support the findings of the study are available from the corresponding author upon request.

Conflicts of Interest

The authors declare that they have no conflicts of interest.

References

[1] Renewables 2017: Global Status Report. 2017.

[2] J.-I. Lee, I.-W. Lee, and S.-H. Kim, "Multi-site photovoltaic power generation forecasts based on deep-learning algorithm," in *Proceedings of the 2017 International Conference on Information and Communication Technology Convergence (ICTC)*, pp. 1118–1120, Jeju, South Korea, 2017.

[3] J. Antonanzas, N. Osorio, R. Escobar, R. Urraca, F. J. Martinez-de-Pison, and F. Antonanzas-Torres, "Review of photovoltaic power forecasting," *Solar Energy*, vol. 136, pp. 78–111, 2016.

[4] S. Sobri, S. Koohi-Kamali, and N. A. Rahim, "Solar photovoltaic generation forecasting methods: a review," *Energy Conversion and Management*, vol. 156, pp. 459–497, 2018.

[5] R. H. Inman, H. T. C. Pedro, and C. F. M. Coimbra, "Solar forecasting methods for renewable energy integration," *Progress in Energy and Combustion Science*, vol. 39, no. 6, pp. 535–576, 2013.

[6] C. Voyant, G. Notton, S. Kalogirou et al., "Machine learning methods for solar radiation forecasting: a review," *Renewable Energy*, vol. 105, pp. 569–582, 2017.

[7] M. Zamo, O. Mestre, P. Arbogast, and O. Pannekoucke, "A benchmark of statistical regression methods for short-term forecasting of photovoltaic electricity production. Part II: probabilistic forecast of daily production," *Solar Energy*, vol. 105, pp. 804–816, 2014.

[8] F. Almonacid, P. J. Pérez-Higueras, E. F. Fernández, and L. Hontoria, "A methodology based on dynamic artificial neural network for short-term forecasting of the power output of a PV generator," *Energy Conversion and Management*, vol. 85, pp. 389–398, 2014.

[9] Y. Chu, B. Urquhart, S. M. I. Gohari, H. T. C. Pedro, J. Kleissl, and C. F. M. Coimbra, "Short-term reforecasting of power output from a 48 MWe solar PV plant," *Solar Energy*, vol. 112, pp. 68–77, 2015.

[10] Z. Li, S. Rahman, R. Vega, and B. Dong, "A hierarchical approach using machine learning methods in solar photovoltaic energy production forecasting," *Energies*, vol. 9, no. 1, p. 55, 2016.

[11] L. Gigoni, A. Betti, E. Crisostomi et al., "Day-ahead hourly forecasting of power generation from photovoltaic plants," *IEEE Transactions on Sustainable Energy*, vol. 9, no. 2, pp. 831–842, 2018.

[12] Y. Zhang, M. Beaudin, R. Taheri, H. Zareipour, and D. Wood, "Day-ahead power output forecasting for small-scale solar photovoltaic electricity generators," *IEEE Transactions on Smart Grid*, vol. 6, no. 5, pp. 2253–2262, 2015.

[13] K. E. Taylor, "Summarizing multiple aspects of model performance in a single diagram," *Journal of Geophysical Research: Atmospheres*, vol. 106, no. D7, pp. 7183–7192, 2001.

[14] J. Kleissl, Ed., *Solar Energy Forecasting and Resource Assessment*, Elsevier, Amsterdam, Netherlands, 1st edition, 2013.

[15] T. Markvart, *Solar Electricity*, John Wiley & Sons, Hoboken, NJ, USA, 2000.

[16] T. Camacho-Lopez, *Sandia Energy*, PV Publications, Stevenage, UK, 2019, https://energy.sandia.gov/energy/renewable-energy/solar-energy/photovoltaics/publications/.

[17] A. D. Jones and C. P. Underwood, "A modelling method for building-integrated photovoltaic power supply," *Building Services Engineering Research and Technology*, vol. 23, no. 3, pp. 167–177, 2002.

[18] A. El Hendouzi and A. Bourouhou, "Forecasting of PV power application to PV power penetration in a microgrid," in *Proceedings of the 2016 International Conference on Electrical and Information Technologies (ICEIT)*, pp. 468–473, Tangiers, Morocco, 2016.

[19] A. H. Murphy, "Skill scores based on the mean square error and their relationships to the correlation coefficient," *Monthly Weather Review*, vol. 116, no. 12, pp. 2417–2424, 1988.

[20] "JRC photovoltaic geographical information system(PVGIS)—European commission" 2019, http://re.jrc.ec.europa.eu/pvg_tools/en/tools.html#TMY.

Hindawi
Journal of Electrical and Computer Engineering
Volume 2020, Article ID 6382507, 11 pages
https://doi.org/10.1155/2020/6382507

Research Article

Optimal Reactive Power Flow for Large-Scale Power Systems Using an Effective Metaheuristic Algorithm

Thanh Long Duong,[1] **Minh Quan Duong**,[2] **Van-Duc Phan**,[3] **and Thang Trung Nguyen**[4]

[1]*Faculty of Electrical Engineering Technology, Industrial University of Ho Chi Minh City, Ho Chi Minh City, Vietnam*
[2]*Electrical Engineering Faculty, The University of DaNang, University of Science and Technology, DaNang City, Vietnam*
[3]*Faculty of Automobile Technology, Van Lang University, Ho Chi Minh City 700000, Vietnam*
[4]*Power System Optimization Research Group, Faculty of Electrical and Electronics Engineering, Ton Duc Thang University, Ho Chi Minh City 700000, Vietnam*

Correspondence should be addressed to Thang Trung Nguyen; nguyentrungthang@tdtu.edu.vn

Received 20 August 2019; Revised 7 January 2020; Accepted 13 January 2020; Published 1 March 2020

Guest Editor: Alessandro Niccolai

Copyright © 2020 Thanh Long Duong et al. This is an open access article distributed under the Creative Commons Attribution License, which permits unrestricted use, distribution, and reproduction in any medium, provided the original work is properly cited.

In this paper, stochastic fractal search method (SFS) is employed for solving the optimal reactive power flow (ORPF) problem with a target of optimizing total active power losses (TPL), voltage deviation (VD), and voltage stability index (VSI). SFS is an effective metaheuristic algorithm consisting of diffusion process and two update processes. ORPF is a complex problem giving challenges to applied algorithms by taking into account many complex constraints such as operating voltage from generators and loads, active and reactive power generation of generators, limit of capacitors, apparent power limit from branches, and tap setting of transformers. For verifying the performance, solutions of IEEE 30 and 118-bus system with TPL, VD, and VSI objectives are found by the SFS method with different control parameter settings. Result comparisons indicate that SFS is more favorable than other methods about finding effective solutions and having faster speed. As a result, it is suggested that SFS should be used for ORPF problem, and modifications performed on SFS are encouraged for better results.

1. Introduction

In the power system, optimal reactive power flow (ORPF) is not only one of the best famous optimization problems but also a very complex problem. In the ORPF problem, two variables need to be considered such as control variables and dependent variables. Control variables are voltage of generation buses, on load tap-changer setting of transformers and generated reactive power of capacitor banks, while dependent variables are voltage of load buses, apparent power flow of transmission lines, and reactive power of generators. So, the major objectives of such ORPF problem is to find control variable so that others have values falling into a permitted operating range [1, 2]. Traditionally, the ORPF problem concentrates on reducing three individual objectives such as power losses of transmission lines, voltage deviation, and voltage stability index. So, a power system economically and stably operates when these goals are fully achieved.

In the last decades of the 20th century, the ORPF problem has been successfully addressed by many conventional methodologies called deterministic methodologies such as the Newton method [3], linear programming [4–7], interior point method [8, 9], quadratic programming method [10, 11], and dynamic programming method [12]. With appearance of the mentioned methods, they proved their strong points in dealing with the ORPF problem having linear constraints and differentiable functions for application, but a large system or more complicated constraints and their applicability must be stopped to make rooms for new methods which have a promising ability.

Luckily, developing computer science supported researchers much in creating new population-based methods to handle drawbacks of conventional methods. These

methods have been successfully and widely applied to solving the ORPF problem, consisting many original methods, improve/modified methods, or combined/hybrid methods. They have been constantly developed and have become a big method family such as particle swarm optimization (PSO) family [13–17], differential evolution (DE) family [18–21], and genetic algorithm (GA) family [22–25], while many standard methods have been also applied in [26–34]. Sahli et al. [16] presented a combination between particle swarm optimization and tabu search (PSO-TS) by incorporating the best search function of PSO and TS. It was capable of finding the global solution and avoiding to fall into local optimum. By the way of evaluation of results attained from the standard IEEE 30-bus system with objective of power loss minimization, PSO-TS has seen better solution quality than other methods as conventional DE, PSO, and TS. Furthermore, a modified version of PSO called modified pseudogradient search-particle swarm optimization (MPG-PSO) has been proposed in [17]. MPG-PSO has the most powerful ability in the PSO family due to applying pseudogradient theory for determining the best velocity direction. As a result, the method has overtaken other PSO methods involving PSO using the time-varying inertia weight factor (PSO-TVIW), PSO using time-varying acceleration coefficients (PSO-TVAC), self-organizing particle swarm optimization using time-varying acceleration coefficients (SPSO-TVAC), PSO using constriction factor (PSO-CF), pseudogradient-based PSO (PG-PSO), PSO using stochastic weight trade-off factor (SWT-PSO), and SWT-PSO using pseudogradient method (PGSWT-PSO). Differential evolution (DE) family has been offered for ORPF-like traditional differential evolution (DE), hybrid ant system and differential evolution method (HAS-DE) [20], and hybrid double differential evolution technique and modified teaching learning technique (DDET-MTLT) [21]. In [20], Huang and Huang have replaced the selection operation of DE by the ant system to enhance the global search capability and avoid falling into local minima and decrease computational time. DDET-MTLT [21] was a combination of double differential evolution technique (DDET) and modified teaching learning technique (MTLT). The obtained results of DDET-MTLT have been compared to some methods on IEEE-30 and IEEE 118-bus systems. Besides, variants of genetic algorithm have been applied for ORPF such as genetic algorithm (GA) [22], enhanced genetic algorithm (EGA) [23], modified NSGA-II (MNSGA-II) [24], self-adaptive real coded genetic algorithm (SARCGA) [25], and hybrid evolutionary programming technique HEP [25].

In addition to the three above method family, other standard methodologies have been also applied for solving ORPF problem such as gravitational search algorithm (GSA) [26], ant lion optimizer (ALO) [27], quasi-oppositional teaching learning based optimization (QOTLBO) [28], teaching learning based optimization (TLBO) [28], Pooled-neighbor swarm intelligence algorithm (PNSA) [29], hybrid Nelder–Mead simplex-based firefly algorithm (HFA-NMS) [30], chaotic krill herd algorithm (CKHA) [31], artificial bee colony algorithm (ABC) [32], exchange market algorithm (EMA) [33], backtracking search algorithm (BTSA) [34], and harmony search algorithm (HSA) [35]. In summary, all methods have demonstrated their qualification for addressing almost constraints of ORPF problem with acceptable solutions.

In this article, we present a standard stochastic fractal search (SFS) with the goal determining minimization of three different individual objectives of ORPF problem such as minimizing TPL, reducing of VD, and enhancing VSI. The standard stochastic fractal search [36] was developed in 2014 by Salimi. It has been applied for addressing twenty-three standard benchmark functions and has proven its proficiency in finding optimal solutions better than many methods available in this literature. In [37], Tran at al. have applied an improved SFS (ISFS) method and SFS method for dealing with the ORPF problem. Only the IEEE 30-bus system with three objectives consisting of total power losses, voltage deviation and L-index have been employed for comparing and evaluating the real performance of the SFS method and ISFS method. From the minimum, average, and maximum fitness functions obtained from the three objectives, ISFS has been considered to be more effective than the SFS method. However, Tran at al. [37] have not taken the setting of control parameters into account. In fact, SFS has three important control parameters consisting of walk factor, population size, and the maximum number of iterations. Among the three parameters, the walk factor has high impact on working performance of the diffusion process; meanwhile, population size has high contribution to the first update and the second update processes. So, in this paper, we focus on the setting of control parameters to overcome such mentioned shortcoming of the work in [37]. Furthermore, we also expand study cases by considering both IEEE 30-bus system and IEEE 118-bus system with the three mentioned objectives. As a result, the novelty and the main contribution of the paper are as follows:

(i) Finding optimal solutions for IEEE 30-bus and 118-bus transmission power networks of ORPF problem by using the SFS method

(ii) Testing the real performance of the SFS method with the change of population size and iterations

(iii) Tuning the best walk factor for determining more appropriate equation for diffusion of the SFS method

(iv) Illustrating the fluctuations of search process of SFS method with different settings;the simulation can support to evaluate the real performance of SFS and the impact of each parameter on the real performance of the SFS method

(v) Demonstrating the effectiveness and robustness of the SFS method by comparing total power losses, load bus voltage, and enhancement of voltage profile

Apart from the introduction, other parts of the paper are as follows: single objective functions and constraints of electric components are mathematically formulated in Section 2. The structure of the SFS method consisting of diffusion and the first and the second update techniques are described in detail in Section 3. Computation steps of solving ORPF problem by using the SFS method are shown in

Section 4. The results obtained by SFS and other methods from two standard IEEE transmission power networks with 30 buses and 118 buses are compared and discussed in Section 5. The whole work of the paper is summarized in and concluded in Section 6.

2. Formulation of ORPF Problem

The ORPF problem is constructed by considering minimization of total active power losses (P_{loss}), reduction of load bus voltage deviation (VD), and enhancement of voltage stability as objectives and taking into account operating voltage of generators and loads, apparent power limit of branches, reactive power generation of generators, and active and reactive power balance equations. The structure of ORPF problem is described in detail as follows.

2.1. Objectives of ORPF Problem. Three main objectives of the ORPF problem considered in the paper consist of minimization of total active power losses, minimization of voltage deviation at load buses, and minimization of L-index in which minimization of L-index is corresponding to the enhancement of voltage stability. The three objectives can be seen in formulas (1)–(3) as follows:

$$\text{Minimize} \sum P_{\text{loss}} = \sum_{i=1}^{N_{\text{bus}}} \sum_{\substack{j=1 \\ j \neq i}}^{N_{\text{bus}}} G_{ij} \left[V_i^2 + V_j^2 - 2V_i V_j \cos\left(\beta_i - \beta_j\right) \right], \tag{1}$$

$$\text{Minimize VD} = \sum_{i=1}^{N_{\text{load}}} \left| V_{\text{loadi}} - V_{\text{ref}} \right|, \tag{2}$$

$$\text{Minimize L} - \text{index} = \max\left(L_j\right); \quad j = 1, \ldots, N_{\text{bus}}, \tag{3}$$

where G_{ij} is the conductance of conductor ij; β_i and β_j are the phases of voltage at buses i and j, respectively; V_{loadi} is the voltage of load bus i; V_{ref} is expected to be the voltage equaling 1.0 pu; and L_j is called L-index of-bus j [16].

Basically, L-index is within the range from 0 to 1 in which 0 is the best value and 1 is the worst value. The power system is considered to be working stably when L-index is close to 0, and it is working unstably or it will be collapsed in some seconds if L-index is close to 1. So, the main task to keep the power system working stably and economically is to reduce L-index close to 0. However, it is hard to tune control parameter for obtaining 0 value for L-index.

2.2. Constraints of ORPF Problem. ORPF are constrained by equality and inequality constraints covering the whole transmission power network. The equality constraints are considering active and reactive power balance while the inequality constraints are upper and lower limitations of electricity components and working parameters of power network.

The two equality constraints are as follows:

$$P_{Gi} - P_{di} = V_i \sum_{j=1}^{N_{\text{bus}}} V_j \left[g_{ij} \cos\left(\beta_i - \beta_j\right) + b_{ij} \sin\left(\beta_i - \beta_j\right) \right], \tag{4}$$

$$Q_{Gi} + Q_{ci} - Q_{di} = V_i \sum_{j=1}^{N_{\text{bus}}} V_j \left[g_{ij} \sin\left(\beta_i - \beta_j\right) - b_{ij} \cos\left(\beta_i - \beta_j\right) \right]. \tag{5}$$

where g_{ij} and b_{ij} are real and unreal terms of admittance of conductor ij, respectively. The inequality constraints are limitations of reactive power output and voltage of generators, the reactive power output of capacitors, tap values of transformers, voltage of load buses, and apparent power of lines. All the inequality constraints are as follows:

$$Q_{Gi,\min} \leq Q_{Gi} \leq Q_{Gi,\max}; \quad i = 1, \ldots, N_G, \tag{6}$$

$$V_{Gi,\min} \leq V_{Gi} \leq V_{Gi,\max}; \quad i = 1, \ldots, N_G, \tag{7}$$

$$Q_{ci,\min} \leq Q_{ci} \leq Q_{ci,\max}; \quad i = 1, \ldots, N_c, \tag{8}$$

$$T_{i,\min} < T_i < T_{i,\max}; \quad i = 1, \ldots, N_t, \tag{9}$$

$$V_{\text{loadi},\min} \leq V_{\text{loadi}} \leq V_{\text{loadi},\max}; \quad i = 1, \ldots, N_{\text{load}}, \tag{10}$$

$$S_l \leq S_{l,\max}; \quad l = 1, \ldots, N_{\text{branch}}. \tag{11}$$

3. Stochastic Fractal Search Algorithm

3.1. Diffusion Technique. SFS is an improved version of fractal search and was developed by Salimi in 2014 [36]. SFS is constructed by three main processes including diffusion and two different update processes. Consequently, SFS has three new solution generations in each iteration in which the diffusion process plays the most important role. The diffusion process uses Gaussian random walk for generating new solutions as follows:

$$X_{s,\text{new}}^1 = \text{Gaussian}\left(G_{\text{best}}, \sigma\right) + \text{rand} \times \left(G_{\text{best}} - X_s\right), \tag{12}$$

$$X_{s,\text{new}}^1 = \text{Gaussian}\left(X_s, \sigma\right), \tag{13}$$

$$\sigma = \left| \frac{\log(\text{CI})}{\text{CI}} \times \left(X_s - G_{\text{best}}\right) \right|, \tag{14}$$

where G_{best} is the best solution among the set of points. CI is the current iteration.

As seen from equations (12) and (13), the diffusion process can be accomplished by using either equations (12) or (13) meanwhile the two equations have a major difference. Equation (12) uses Gaussian random walk around the best solution and an updated step by using $(G_{\text{best}} - X_s)$ while equation (13) only employs random walk around X_i. Due to the difference, SFS must propose one more control parameter, called walk factor (WF) to control the use of either equations (12) or (13). The walk factor is compared to a

random number and the result will lead to a decision of used equation. If walk factor is higher than the random number, equation (12) is employed for producing new solution for the sth solution. Otherwise, equation (13) is selected. The diffusion technique can be performed by using Algorithm 1.

3.2. Second Update Technique. The first update is the second new solution generation and is performed by the following equation:

$$X^2_{s,\text{new}} = X_{\text{random1}} - \text{rand} \times \left(X_{\text{random2}} - X_s\right), \tag{15}$$

where X_{random1} and X_{random2} are solutions chosen randomly in the current set of solutions and $X^2_{s,\text{new}}$ is the new solution of solution X_s.

3.3. Third Update Technique. After implementing the first update, the second update equivalent to the third new solutions is carried out for updating solutions of the second generation and is expressed by

$$X^3_{s,\text{new}} = \begin{cases} X^2_{s,\text{new}} - \text{rand} \times \left(X_{\text{random1}} - G_{\text{best}}\right), & \text{for } RN_s \le 0.5 \\ X^2_{s,\text{new}} + \text{rand} \times \left(X_{\text{random2}} - X_{\text{random3}}\right), & \text{for } RN_s > 0.5 \end{cases} \tag{16}$$

where X_{random1}, X_{random2}, and X_{random3} are three random solutions chosen from the current set and RN_s is a random number ranging from 0 to 1 for solution s.

4. Implementation of SFS for ORPF Problem

4.1. Initialization. The ORPF problem can be solved by using mathpower 4.1 programming after a set of control variables is predetermined by the SFS problem. In fact, the control variable set that has to be inserted into the program is the voltage of thermal generators (V_{G1}, ..., V_{GNG}), tap values of transformers (T_1, ..., T_{Nt}), and reactive power output of capacitor banks (Q_{c1}, ..., Q_{cNc}). Thus, each point (corresponding to each solution) of the SFS method must represent all the variables and is randomly produced as follows:

$$X_s = X_{\min} + \text{rand} \times \left(X_{\max} - X_{\min}\right); \quad s = 1, ..., N_{\text{pop}}, \tag{17}$$

where $X_{\min}$ and $X_{\max}$ are the lowest and highest values of such control variables.

4.2. Fitness Function. As a result, the fitness function is constructed equaling the sum of objective function and penalty terms [17]. For three single objective functions including total power loss, voltage deviation, and L-index, three corresponding fitness functions are formulated as follows:

$$\begin{aligned} \text{FF}_s &= \sum P_{\text{loss}} + \text{VPF} \cdot \left(\Delta Q_{Gi} + \Delta V_{\text{loadi}} + \Delta S_l\right)^2, \\ \text{FF}_s &= \text{VD} + \text{VPF} \cdot \left(\Delta Q_{Gi} + \Delta V_{\text{loadi}} + \Delta S_l\right)^2, \\ \text{FF}_s &= \text{L} - \text{index} + \text{VPF} \cdot \left(\Delta Q_{Gi} + \Delta V_{\text{loadi}} + \Delta S_l\right)^2. \end{aligned} \tag{18}$$

```
Set a value to WF
For s = 1 to N_pop
    Randomly produce a random number λ_s for the
    sth solution
    If WF is higher than λ_s
        Using equation (12) for updating the
        sth new solution
    Else
        Using equation (13) for updating the
        sth new solution
    End
end
```

Algorithm 1: Diffusion technique for the first generation of new solutions.

where $\sum P_{\text{loss}}$, VD and L-index are obtained by using equations (1)–(3), VPF is the penalty factor for the violation of the dependent variable, and ΔQ_{Gi}, ΔV_{loadi}, and ΔS_l are penalty terms corresponding to the violation of Q_{Gi} in constraint (6), V_{loadi} in constraint (10), and S_l in constraint (11).

The penalty terms are determined by

$$\begin{aligned} \Delta Q_{Gi} &= \begin{cases} 0, & \text{if } Q_{Gi,\min} < Q_{Gi} < Q_{Gi,\max}, \\ \left(Q_{Gi,\min} - Q_{Gi}\right), & \text{if } Q_{Gi,\min} \ge Q_{Gi}, \\ \left(Q_{Gi} - Q_{Gi,\max}\right)^2, & \text{if } Q_{Gi,\max} \le Q_{Gi}, \end{cases} \\ \Delta V_{loadi} &= \begin{cases} 0, & \text{if } V_{\text{loadi},\min} < V_{\text{loadi}} < V_{\text{loadi},\max}, \\ \left(V_{\text{loadi},\min} - V_{\text{loadi}}\right), & \text{if } V_{\text{loadi},\min} \ge V_{\text{loadi}}, \\ \left(V_{\text{loadi}} - V_{\text{loadi},\max}\right)^2, & \text{if } V_{\text{loadi},\max} \le V_{\text{loadi}}, \end{cases} \\ \Delta S_l &= \begin{cases} 0, & \text{if } S_l \le S_{l,\max}, \\ \left(S_l - S_{l,\max}\right), & \text{else.} \end{cases} \end{aligned} \tag{19}$$

4.3. Termination Condition. The three main processes of the SFS method will be terminated when current iteration (CI) is equal to the maximum iteration (MI), which is predetermined initially.

5. Numerical Results

In the section, we test the performance of the SFS method for the ORPF problem with two systems having 30 buses and 118 buses under considering three objectives such as power loss, voltage deviation, and L-index. The method is executed on Matlab program language and a computer with the processor of Core i7, 2.4 GHz, and 4 GB of RAM.

5.1. Results Obtained on IEEE 30-Bus System. In the section, we implement the SFS method for optimizing total power losses, voltage deviation, and L-index of the IEEE 30-bus

system by setting different values to control parameters such as population size, maximum iteration, and walk factor. The IEEE 30-bus system consists of 6 generators, 24 loads, and 41 branches, 9 VAR compensators, and 4 transformers [38]. In order to indicate the impact of control parameters on results, we perform three testing cases as follows:

(1) The first testing case: tune different values for population size while fixing the maximum iteration at value of 200

(2) The second testing case: tune different values for the maximum iteration while fixing population size to the best value obtained by the first testing case

(3) The third testing case: tune different values for walk factor while fixing population size and the maximum iteration at the best value obtained by the first testing case and the second testing case

The three testing cases are presented in Section 5.1.1, while the comparison of results from SFS method and other ones is shown in Section 5.1.2 and Section 5.2.

5.1.1. Analysis of Control Parameters on Results Obtained by SFS Method. The results in terms of the best, mean, worst power losses, standard deviation, and simulation time for each run (ST) are shown in Tables 1–3 corresponding to the first, second, and third testing cases. The results from Table 1 indicate that population size of 10 is high enough for finding the best solution while increasing the population size to 15 and 20 cannot find a better solution but average and maximum power losses can be improved whereas simulation time is increased. Figure 1 also gives the same evaluation since the curve in blue has high number of solutions with better fitness than other curves.

Table 2 show the results obtained by setting different values to the maximum iteration while keeping the population size at 10. The maximum iteration is increased from 50 to 250 with a step of 50. The best power loss implies that SFS method can find the best solution at different values of the maximum iteration such as 200 and 250; meanwhile, smaller number of iterations cannot reach the same best solution. The best optimal solution of MI = 200 and MI = 250 has the same quality; meanwhile, the mean fitness function value of 50 runs from MI = 250 is smaller. In spite of the advantage of MI = 250, SFS should adopt the most appropriate number of iterations is 200 because it can find as good as solution but it can reduce simulation time. Figure 2 shows that the curve in blue has many solutions with the same fitness as those from curve in black.

From Tables 1 and 2 as well as from Figures 1 and 2, it can result in the selection of population size and the maximum iteration in which the best value of the comer is 10 while the most appropriate value of the later is 200. By using the two values, walk factor's impact on performance of the SFS method is tried by setting it to 0, 0.2, 0.4, 0.6, 0.8, and 1. Table 3 and Figure 3 show that the walk factor to be 1 is the best value for reaching the best solution, whereas other values cannot reach the same best solution. As observing from the best power loss, the walk factor with higher value can support the SFS method find superior solutions. In fact, power loss is the highest at WF = 0, and it decreases since the factor approaches to 1. So, it can conclude that diffusion technique becomes more effective if equation (12) is used to replace equation (13).

5.1.2. Result Comparisons for IEEE 30-Bus System. The results in terms of minimum, average, maximum, and standard deviation accompany with control parameters including MI and N_{pop} from SFS and other methods are reported in Tables 4–6 for power loss, voltage deviation, and L-index, respectively. Besides, saving percentage (%) of the SFS method compared with each one is also calculated and reported in the tables for further comparisons. Saving percentage from these tables can see that SFS outperforms most methods excluding PSO-TS [16] and ISFS [37] for power loss objective and QOTLBO [28] for voltage deviation objective. Saving values show that these methods get improvement over SFS by 0.137%, 0.295%, and 2.45%; however, only ISFS [37] has found better solution than SFS, meanwhile PSO-TS [16] has not reported MI and N_{pop} for comparison of convergence speed and recalculated minimum of QOTLBO is 0.1031, which is much higher than reported value of 0.0856. Clearly, QOTLBO is less effective than SFS. SFS can get improvement over other methods for power loss optimization from 0.7% to 8.365%, for voltage deviation optimization from 1.68% to 57.51%, and for L-index from 13.26% to 32.82%. Clearly, the improvement is significant and optimal solution of SFS is much better than those from other methods. Furthermore, convergence speed of SFS is also faster or approximate with other compared methods since SFS uses MI = 200, $N_{pop} = 10$, while those from others are 100 and 50, 200 and 20, or MI = 30,000.

Optimal solutions of three optimization cases are given in Table 7.

5.2. Results Obtained on IEEE 118-Bus System. This section uses the IEEE 118-bus system consisting of 54 generator buses, 64 load buses, and 186 transmission lines, 14 VAR compensators, and 9 transformers [37] (Table 8). We implement the SFS method for optimizing total power losses of the system by setting different values to population size and the maximum iteration. In the first trial, we increase the population size from 10 to 100 with a change of 10 and fixing the maximum iteration to 150 and 200. In the second trial, population size is selected to be 50 and 75; meanwhile, the maximum iteration is increased from 50 to 400 with a step of 50. The optimal solution obtained by SFS method is given in Table 9. In addition, the results in terms of the best power loss, mean power loss, and success rate (SR) in percentage are, respectively, shown in Tables 9 and 10. From the two tables, it is clear that SFS can improve search ability since the

Table 1: Results obtained by setting different values to N_{pop}, and fixing MI = 200 and WF = 1.0.

Population size	The best TPL (MW)	Mean TPL (MW)	The worst TPL (MW)	Std. dev. TPL (MW)	ST (s)
5	5.0708	5.2901	6.3250	0.1847	10.2
10	4.5275	4.6732	5.1844	0.1399	19.7
15	4.5275	4.6639	5.1688	0.1370	29.4
20	4.5275	4.6499	5.1430	0.1352	38.2

Table 2: Results obtained by setting different values to MI, and fixing $N_{pop} = 10$ and WF = 1.0.

MI	The best TPL (MW)	Mean TPL (MW)	The worst TPL (MW)	Std. dev. TPL (MW)	ST (s)
50	6.3838	7.1500	8.1395	0.2252	6.2
100	6.2561	7.0070	7.9767	0.2207	12.1
150	4.7539	6.3063	7.2588	0.1876	18.6
200	4.5275	4.6732	5.1844	0.1399	23.9
250	4.5275	4.6078	5.0029	0.1321	30.0

Table 3: Results obtained by setting different values to WF and fixing $N_{pop} = 10$ and MI = 200.

Walk factor (WF)	The best TPL (MW)	Mean TPL (MW)	The worst TPL (MW)	Std. dev. TPL (MW)	ST (s)
0	6.9724	7.1687	7.6936	0.2154	20.2
0.2	5.9854	6.6453	7.6325	0.2129	20.1
0.4	5.5236	6.1780	7.2167	0.1707	19.7
0.6	4.7539	4.7900	5.3659	0.1560	19.6
0.8	4.5366	4.7293	5.7132	0.1430	19.8
1.0	4.5275	4.6732	5.1844	0.1399	19.5

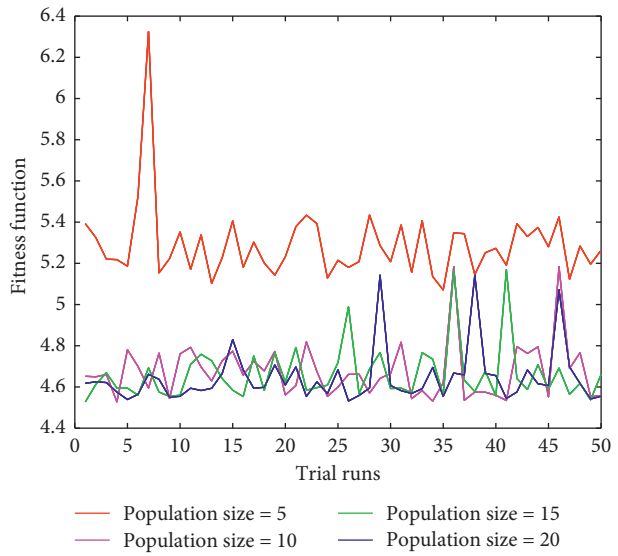

Figure 1: The impact of population size on obtained fitness values of 50 trial runs.

population size and the maximum iteration are increased but simulation time is also increased. 113.021 MW in Table 9 indicates SFS can find the best solution with the setting of $N_{pop} = 60$, 70, 80, 90, and 100, and MI = 150, and $N_{pop} = 50$, 60, 70, 80, 90, and 100 and MI = 200. Clearly, $N_{pop} = 60$ and MI = 150 are the best selection for the case of tuning population size and fixing the maximum iteration. SFS cannot improve result better if the population size is set to higher than 60 for MI = 150 and 70 for MI = 200. Similarly, 113.021 MW in Table 10 indicates that $N_{pop} = 50$ and MI = 200 and $N_{pop} = 75$ and MI = 150 are the best selection for finding the best performance of the SFS method. Improvement of the best solution fails if increasing MI to higher than 200 for $N_{pop} = 50$ and to higher than 150 for

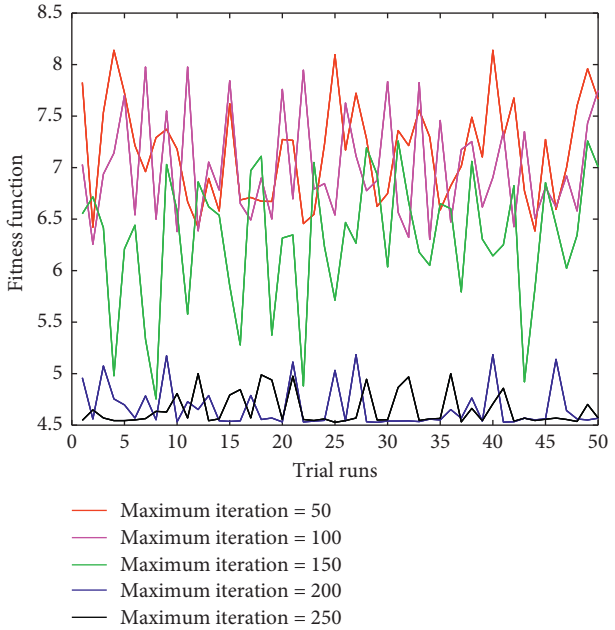

Figure 2: The impact of the maximum iteration on obtained fitness values of 50 trial runs.

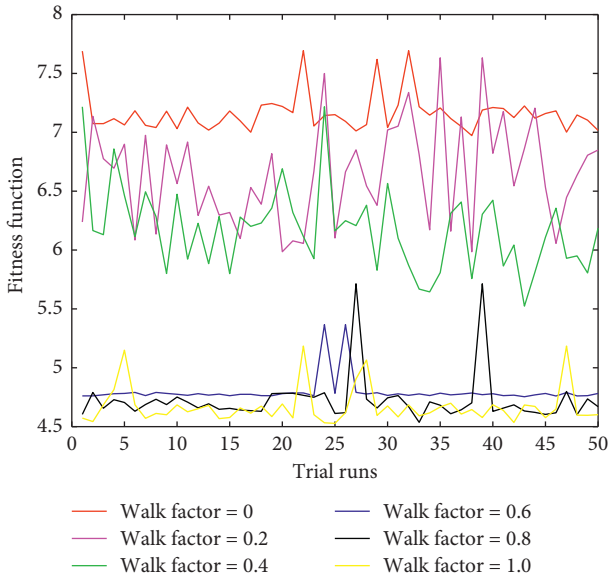

Figure 3: The impact of walk factor on obtained fitness values of 50 trial runs.

Table 4: Comparisons for TPL of the IEEE 30-bus system.

Method	The best TPL (MW)	Mean TPL (MW)	The worst TPL (MW)	Std. dev. TPL (MW)	MI	N_{pop}	Saving percentage (%)
PSO-TS [16]	4.5213	—	—	—	—	—	−0.137
TS [16]	4.9203	—	—	—	—	—	7.983
PSO [16]	4.6862	—	—	—	—	—	3.387
ALO [27]	4.59				100	—	1.362
QOTLBO [28]	4.5594	4.5601	4.5617	0.037	100	50	0.700
TLBO [28]	4.5629	4.5695	4.5748	0.0564	100	50	0.776
SGA [35]	4.9408	5.0378	5.1651	—	30,000	—	8.365
PSO [35]	4.9239	4.972	5.0576	—	30,000	—	8.051
HSA [35]	4.9059	4.924	4.9653	—	30,000	—	7.713
SFS [37]	4.5777	—	—	1.05	100	20	1.097
ISFS [37]	4.5142	—	—	0.012	—	—	−0.295
SFS	4.5275	4.6732	5.1844	0.1399	200	10	

Table 5: Comparisons for VD of the IEEE 30-bus system.

Method	The best VD (pu)	Mean VD (pu)	The worst VD (pu)	Std. dev. VD (pu)	MI	N_{pop}	Saving percentage (%)
PSO-TVIW [17]	0.1038	0.1597	0.5791	0.1112	200	20	15.51
PSO-TVAC [17]	0.2064	0.2376	0.5796	0.0153	200	20	57.51
SPSO-TVAC [17]	0.1354	0.1558	0.1833	0.0103	200	20	35.23
PSO-CF [17]	0.1287	0.1557	0.4041	0.0404	200	20	31.86
PG-PSO [17]	0.1202	0.144	0.2593	0.0222	200	20	27.04
SWT-PSO [17]	0.1614	0.1814	0.2296	0.133	200	20	45.66
PGSWT-PSO [17]	0.1539	0.2189	0.5532	0.0656	200	20	43.01
MPG-PSO [17]	0.0892	0.1078	0.2518	0.0298	200	20	1.68
QOTLBO [28]	0.0856	0.0872	0.0907	0.0314	200	10	−2.45
TLBO [28]	0.0913	0.0934	0.0988	0.0403	100	50	3.94
SFS [37]	0.122	—	—	0.016	100	20	28.115
ISFS [37]	0.089	—	—	0.0031	100	20	1.461
SFS	0.0877	0.1207	0.1577	0.0155	200	10	—

Table 6: Comparisons for VSI of the IEEE 30-bus system.

Method	The best L-index (pu)	Mean L-index (pu)	The worst L-index (pu)	Std. dev. L-index (pu)	MI	N_{pop}	Saving percentage (%)
PSO-TVIW [17]	0.1258	0.127	0.1289	0.0008	200	20	19.95
PSO-TVAC [17]	0.1499	0.1513	0.1544	0.0009	200	20	32.82
SPSO-TVAC [17]	0.1271	0.1285	0.1297	0.0006	200	20	20.77
PSO-CF [17]	0.1261	0.1279	0.1295	0.0008	200	20	20.14
PG-PSO [17]	0.1264	0.1297	0.1313	0.0008	200	20	20.33
SWT-PSO [17]	0.1488	0.1634	0.1806	0.0074	200	20	32.33
PGSWT-PSO [17]	0.1394	0.1537	0.1749	0.0081	200	20	27.76
MPG-PSO [17]	0.1241	0.1266	0.1298	0.001	200	20	18.86
BA [27]	0.1191	—	—	—	100	40	15.45
GWO [27]	0.118	—	—	—	100	40	14.66
ABC [27]	0.1161	—	—	—	100	40	13.26
ALO [27]	0.1161	—	—	—	100	40	13.26
QOTLBO [28]	0.1242	0.1245	0.1247	0.0452	100	50	18.92
TLBO [28]	0.1252	0.1254	0.1258	0.0454	100	50	19.57
SFS [37]	0.1252	—	—	0.021	100	20	19.569
ISFS [37]	0.1245	—	—	0.004	100	20	19.116
SFS	0.1007	0.1043	0.1138	0.0026	200	10	—

Table 7: Optimal solutions of the IEEE 30-bus system.

Variable	TPL objective	VD objective	L-index objective
V_{G1}	1.1000	1.0055	1.0807
V_{G2}	1.0952	1.0011	1.0538
V_{G5}	1.0750	1.0173	1.0739
V_{G8}	1.0765	1.0120	1.0089
V_{G11}	1.0873	1.0320	1.0801
V_{G13}	1.0999	1.0234	1.0851
T_1	1.0500	1.0500	0.9000
T_2	0.9200	0.9000	0.9000
T_3	1.0100	1.0000	0.9000
T_4	0.9800	0.9700	0.9000
Q_{c1}	5.0000	4.0000	5.0000
Q_{c2}	5.0000	2.0000	5.0000
Q_{c3}	5.0000	4.0000	0.0000
Q_{c4}	5.0000	3.0000	0.0000
Q_{c5}	3.0000	5.0000	5.0000
Q_{c6}	5.0000	3.0000	3.0000
Q_{c7}	3.0000	5.0000	5.0000
Q_{c8}	4.0000	5.0000	5.0000
Q_{c9}	2.0000	3.0000	1.0000

Table 8: Optimal solution of the IEEE 118-bus transmission power network.

V_{G1} (pu)	1.0081	V_{G62}	1.0223	V_{G113}	1.005
V_{G4}	1.0439	V_{G65}	1.0563	V_{G116}	1.0379
V_{G6}	1.0376	V_{G66}	1.051	T_8 (pu)	0.9762
V_{G8}	1.0081	V_{G69}	1.0574	T_{32}	1.0192
V_{G10}	1.0267	V_{G70}	1.0308	T_{36}	1.0031
V_{G12}	1.0309	V_{G72}	1.0204	T_{51}	0.9785
V_{G15}	1.004	V_{G73}	1.0374	T_{93}	0.9981
V_{G18}	1.0021	V_{G74}	1.0043	T_{95}	1.0081
V_{G19}	0.9992	V_{G76}	0.989	T_{102}	1.0132
V_{G24}	1.0069	V_{G77}	1.0298	T_{107}	0.9963
V_{G25}	1.0436	V_{G80}	1.0471	T_{127}	0.9821
V_{G26}	1.0356	V_{G85}	1.0349	Q_{C5} (MVAR)	−2.349
V_{G27}	1.0366	V_{G87}	0.9944	Q_{C34}	7.4927
V_{G31}	1.023	V_{G89}	1.0764	Q_{C37}	−16.55
V_{G32}	1.0212	V_{G90}	1.0575	Q_{C44}	6.8138
V_{G34}	1.0266	V_{G91}	1.0464	Q_{C45}	3.8515
V_{G36}	1.0244	V_{G92}	1.0515	Q_{C46}	5.0318
V_{G40}	1.0371	V_{G99}	1.0285	Q_{C48}	7.1142
V_{G42}	1.0388	V_{G100}	1.0516	Q_{C74}	5.985
V_{G46}	1.0173	V_{G103}	1.0361	Q_{C79}	10.574
V_{G49}	1.0469	V_{G104}	1.0148	Q_{C82}	14.366
V_{G54}	1.0366	V_{G105}	1.0133	Q_{C83}	6.8917
V_{G55}	1.0321	V_{G107}	1.0265	Q_{C105}	6.4333
V_{G56}	1.0328	V_{G110}	1.0201	Q_{C107}	2.3679
V_{G59}	1.0388	V_{G111}	1.0197	Q_{C110}	5.3222
V_{G61}	1.0221	V_{G112}	1.0261		

Table 9: Result obtained by setting MI = 150, MI = 200 and different values for population size.

N_{pop}	MI = 150				MI = 200			
	The best TPL (MW)	Mean TPL (MW)	SR (%)	ST (s)	The best TPL (MW)	Mean TPL (MW)	SR (%)	ST (s)
10	161.620	206.233	15	46	156.772	193.034	18.69	61
20	154.186	196.747	25	90	149.560	184.155	31.15	119
30	145.552	187.696	47	126	141.185	175.684	54	163
40	135.945	179.062	54	181	131.867	167.602	61	239
50	122.894	159.423	65	226	113.021	149.220	75	302
60	**113.021**	134.793	88	275	113.021	126.166	89	354
70	113.021	130.075	92	317	113.021	121.750	94	422
80	113.021	125.783	95	359	113.021	124.651	96	477
90	113.021	121.758	94	402	113.021	120.662	98	534
100	113.021	117.618	95	449	113.021	116.559	98	572

Table 10: Result obtained by setting $N_{pop} = 50$ and $N_{pop} = 75$ and different values for the maximum iterations.

MI	$N_{pop} = 50$				$N_{pop} = 75$			
	The best TPL (MW)	Mean TPL (MW)	SR (%)	ST (s)	The best TPL (MW)	Mean TPL (MW)	SR (%)	ST (s)
50	154.308	212.230	12	72	124.323	198.647	25	107
100	125.454	202.467	54	147	119.124	189.510	69	221
150	119.011	193.154	77	226	**113.021**	130.221	82	340
200	**113.021**	131.027	91	293	113.021	121.887	90	437
250	113.021	129.590	93	365	113.021	121.107	92	545
300	113.021	126.856	95	438	113.021	120.545	94	656
350	113.021	123.036	97	511	113.021	114.952	96	768
400	113.021	119.578	98	583	113.021	114.648	96	876

$N_{pop} = 75$. So, it can conclude that the best selection for population size and the maximum iterations are $N_{pop} = 60$ and MI = 150. The results from the setting are reported for comparisons with other methods shown in Table 11. The saving percentage of SFS compared with other methods is from 0.09% to 9.1%, while SFS is only less effective than QOTLBO [28] by −0.66%. The comparison indication can conclude that optimal solution of SFS is the second best

Table 11: Comparisons for TPL of the IEEE 118-bus system.

Method	The best TPL (MW)	Mean TPL (MW)	The worst TPL (MW)	Std. dev. TPL (MW)	MI	N_{pop}	Saving percentage (%)
PSO-TVIW [17]	116.8976	118.234	126.6222	1.6009	200	40	3.32
PSO-TVAC [17]	124.3335	129.749	134.1254	2.156	200	40	9.10
SPSO-TVAC [17]	116.2026	117.355	118.139	0.4696	200	40	2.74
PSO-CF [17]	115.6469	116.986	119.8378	0.8655	200	40	2.27
PG-PSO [17]	116.6075	119.396	127.0772	2.107	200	40	3.08
SWT-PSO [17]	124.1476	129.371	141.6147	3.309	200	40	8.96
PGSWTPSO [17]	119.427	122.781	125.762	1.2455	200	40	5.36
MPG-PSO [17]	115.06	116.462	118.35	0.528	200	40	1.77
SARCGA [25]	113.12	113.968	—	0.0002	300	15	0.09
HEP [25]	115.58	115.8	—	0.0018	300	15	2.21
QOTLBO [28]	112.2789	113.769	115.4516	0.0244	100	50	−0.66
TLBO [28]	116.4003	121.390	118.4427	0.0482	100	50	2.90
SFS	113.0213	134.793	233.4538	2.91894	150	60	

among all compared methods. Furthermore, search speed of SFS is in the fastest group once MI and N_{pop} are, respectively, 150 and 60, while those from others are 200 and 40, 300 and 15, and 100 and 50. In summary, SFS can find optimal solutions with higher quality than most compared methods; however, compared with some best methods, SFS is also less potential. Consequently, we suggest SFS should be used as an optimization tool for the ORPF problem and it is more promising if SFS is improved by proposing modifications.

6. Conclusion

In the paper, we apply the SFS method for finding optimal solutions of the ORPF problem for different objectives consisting of power loss, voltage deviation, and voltage stability index. Two different power systems with 30 buses and 118 buses are employed for running the SFS method and results found by SFS together with control parameters are compared with those from other methods. As a result, SFS becomes one of the best methods searching the best optimal solutions for each case and its search speed is also faster than most methods. SFS can own the outstanding points, thanks to its construction consisting of three new solution generations, diffusion process, first update process, and the second update process. However, the performance of SFS still copes with constriction, leading to worse results than several methods about solution and speed. Thus, we suggest SFS should be used for finding solutions of the ORPF problem but modifications should be performed on the conventional SFS for improving the search ability.

Abbreviations

N_{bus}: Number of all buses in network
V_i, V_j: Voltage at bus i and bus j
N_{load}: Number of loads
P_{di}, Q_{di}: Active power and reactive power of load i
Q_{ci}: Reactive power generation of capacitor i
N_G: Number of available generators
$Q_{Gi,min}$, $Q_{Gi,max}$: Minimum and maximum limits of reactive power for generator i
$V_{Gi,min}$, $V_{Gi,max}$: Minimum and maximum voltage of generator i, respectively
$Q_{ci,min}$, $Q_{ci,max}$: Minimum and maximum reactive power output of capacitor at bus i
N_c: Number of capacitor buses
$T_{i,min}$, $T_{i,max}$: Minimum and maximum tap changer of transformer at bus i
N_t: Number of transformer buses
$V_{loadi,min}$, $V_{loadi,max}$: Minimum and maximum operating voltage of load i
$S_{l,max}$: Capacity of branch l.

Data Availability

The information of transmission lines and loads in IEEE 30-bus power transmission power network and IEEE 118-bus power transmission power network used to support the finding of this study have been taken from [38].

Conflicts of Interest

The authors declare that there are no conflicts of interest regarding the publication of this paper.

Acknowledgments

This research was funded by Funds for the Science and Technology Development of the University of Danang, under project no. B2019-DN01-19.

References

[1] T. Nguyen, D. Vo, N. Vu Quynh, and L. Van Dai, "Modified Cuckoo search algorithm: a novel method to minimize the fuel cost," *Energies*, vol. 11, no. 6, p. 1328, 2018.

[2] J. Chintam and M. Daniel, "Real-power rescheduling of generators for congestion management using a novel Satin Bowerbird optimization algorithm," *Energies*, vol. 11, no. 1, p. 183, 2018.

[3] D. Sun, B. Ashley, B. Brewer, A. Hughes, and W. Tinney, "Optimal power flow by Newton approach," *IEEE Transactions on Power Apparatus and Systems*, vol. PAS-103, no. 10, pp. 2864–2880, 1984.

[4] O. Alsac, J. Bright, M. Prais, and B. Stott, "Further developments in LP-based optimal power flow," *IEEE Transactions on Power Systems*, vol. 5, no. 3, pp. 697–711, 1990.

[5] G. Opoku, "Optimal power system VAR planning," *IEEE Transactions on Power Systems*, vol. 5, no. 1, pp. 53–60, 1990.

[6] B. Stott and J. Marinho, "Linear programming for power-system network security applications," *IEEE Transactions on Power Apparatus and Systems*, vol. PAS-98, no. 3, pp. 837–848, 1979.

[7] A. M. Chebbo and M. R. Irving, "Combined active and reactive despatch. I. problem formulation and solution algorithm," *IEE Proceedings-Generation, Transmission and Distribution*, vol. 142, no. 4, pp. 393–400, 1995.

[8] S. Granville, "Optimal reactive dispatch through interior point methods," *IEEE Transactions on Power Systems*, vol. 9, no. 1, pp. 136–146, 1994.

[9] E. Rezania and S. M. Shahidehpour, "Real power loss minimization using interior point method," *International Journal of Electrical Power & Energy Systems*, vol. 23, no. 1, pp. 45–56, 2001.

[10] V. H. Quintana and M. Santos-Nieto, "Reactive-power dispatch by successive quadratic programming," *IEEE Transactions on Energy Conversion*, vol. 4, no. 3, pp. 425–435, 1989.

[11] N. Grudinin, "Reactive power optimization using successive quadratic programming method," *IEEE Transactions on Power Systems*, vol. 13, no. 4, pp. 1219–1225, 1998.

[12] F.-C. Lu and Y. Y. Hsu, "Reactive power/voltage control in a distribution substation using dynamic programming," *IEE Proceedings-Generation, Transmission and Distribution*, vol. 142, no. 6, pp. 639–645, 1995.

[13] H. Yoshida, K. Kawata, Y. Fukuyama, S. Takayama, and Y. Nakanishi, "A particle swarm optimization for reactive power and voltage control considering voltage security assessment," *IEEE Transactions on Power Systems*, vol. 15, no. 4, pp. 1232–1239, 2000.

[14] M. A. Abido, "Multiobjective particle swarm optimization for optimal power flow problem," in *Handbook of Swarm Intelligence*, Springer, Berlin, Heidelberg, Germany, 2011.

[15] K. Mahadevan and P. S. Kannan, "Comprehensive learning particle swarm optimization for reactive power dispatch," *Applied Soft Computing*, vol. 10, no. 2, pp. 641–652, 2010.

[16] Z. Sahli, A. Hamouda, A. Bekrar, and D. Trentesaux, "Hybrid PSO-tabu search for the optimal reactive power dispatch problem," in *Proceedings of the IECON 2014-40th Annual Conference of the IEEE Industrial Electronics Society*, Dallas, TX, USA, November 2014.

[17] J. Polprasert, W. Ongsakul, and V. N. Dieu, "Optimal reactive power dispatch using improved pseudo-gradient search particle swarm optimization," *Electric Power Components and Systems*, vol. 44, no. 5, pp. 518–532, 2016.

[18] M. Varadarajan and K. S. Swarup, "Differential evolution approach for optimal reactive power dispatch," *Applied Soft Computing*, vol. 8, no. 4, pp. 1549–1561, 2008.

[19] A. A. A. E. Ela, M. A. Abido, and S. R. Spea, "Differential evolution algorithm for optimal reactive power dispatch," *Electric Power Systems Research*, vol. 81, no. 2, pp. 458–464, 2011.

[20] C.-M. Huang and Y.-C. Huang, "Combined differential evolution algorithm and ant system for optimal reactive power dispatch," *Energy Procedia*, vol. 14, pp. 1238–1243, 2012.

[21] M. Ghasemi, M. M. Ghanbarian, S. Ghavidel, S. Rahmani, and E. Mahboubi Moghaddam, "Modified teaching learning algorithm and double differential evolution algorithm for optimal reactive power dispatch problem: a comparative study," *Information Sciences*, vol. 278, pp. 231–249, 2014.

[22] K. Iba, "Reactive power optimization by genetic algorithm," *IEEE Transactions on Power Systems*, vol. 9, no. 2, pp. 685–692, 1994.

[23] M. S. Kumari and S. Maheswarapu, "Enhanced genetic algorithm based computation technique for multi-objective optimal power flow solution," *International Journal of Electrical Power & Energy Systems*, vol. 32, no. 6, pp. 736–742, 2010.

[24] S. Jeyadevi, S. Baskar, C. K. Babulal, and M. Willjuice Iruthayarajan, "Solving multiobjective optimal reactive power dispatch using modified NSGA-II," *International Journal of Electrical Power & Energy Systems*, vol. 33, no. 2, pp. 219–228, 2011.

[25] P. Subbaraj and P. N. Rajnarayanan, "Optimal reactive power dispatch using self-adaptive real coded genetic algorithm," *Electric Power Systems Research*, vol. 79, no. 2, pp. 374–381, 2009.

[26] S. Duman, Y. Sönmez, U. Güvenç, and N. Yörükeren, "Optimal reactive power dispatch using a gravitational search algorithm," *IET Generation, Transmission & Distribution*, vol. 6, no. 6, pp. 563–576, 2012.

[27] S. Mouassa, T. Bouktir, and A. Salhi, "Ant lion optimizer for solving optimal reactive power dispatch problem in power systems," *Engineering Science and Technology, an International Journal*, vol. 20, no. 3, pp. 885–895, 2017.

[28] B. Mandal and P. K. Roy, "Optimal reactive power dispatch using quasi-oppositional teaching learning based optimization," *International Journal of Electrical Power & Energy Systems*, vol. 53, pp. 123–134, 2013.

[29] C.-x. Guo and B. Zhao, "A pooled-neighbor swarm intelligence approach to optimal reactive power dispatch," *Journal of Zhejiang University-Science A*, vol. 7, no. 4, pp. 615–622, 2006.

[30] A. Khorsandi, A. Alimardani, B. Vahidi, and S. H. Hosseinian, "Hybrid shuffled frog leaping algorithm and Nelder-Mead simplex search for optimal reactive power dispatch," *IET Generation, Transmission & Distribution*, vol. 5, no. 2, pp. 249–256, 2011.

[31] A. Mukherjee and V. Mukherjee, "Solution of optimal reactive power dispatch by Chaotic Krill Herd algorithm," *IET Generation, Transmission & Distribution*, vol. 9, no. 15, pp. 2351–2362, 2015.

[32] K. Rayudu, G. Yesuratnam, and A. Jayalaxmi, "Artificial Bee Colony algorithm for optimal reactive power dispatch to improve voltage stability," in *Proceedings of the 2016 International Conference on Circuit, Power and Computing Technologies (ICCPCT)*, pp. 1–7, Nagercoil, India, March 2016.

[33] A. Rajan and T. Malakar, "Exchange market algorithm based optimum reactive power dispatch," *Applied Soft Computing*, vol. 43, pp. 320–336, 2016.

[34] A. M. Shaheen, R. A. El-Sehiemy, and S. M. Farrag, "Optimal reactive power dispatch using backtracking search algorithm," *Australian Journal of Electrical and Electronics Engineering*, vol. 13, no. 3, pp. 200–210, 2016.

[35] A. H. Khazali and M. Kalantar, "Optimal reactive power dispatch based on harmony search algorithm," *International Journal of Electrical Power & Energy Systems*, vol. 33, no. 3, pp. 684–692, 2011.

[36] H. Salimi, "Stochastic fractal search: a powerful metaheuristic algorithm," *Knowledge-Based Systems*, vol. 75, pp. 1–18, 2015.

[37] H. V. Tran, T. V. Pham, L. H. Pham, N. T. Le, and T. T. Nguyen, "Finding optimal reactive power dispatch solutions by using a novel improved stochastic fractal search optimization algorithm," *Telecommunication Computing Electronics and Control*, vol. 17, no. 5, pp. 2517–2526, 2019.

[38] MATPOWER 4.1 IEEE 30-bus and 118-bus test system, http://www.pserc.cornell.edu/matpower.